Journal of Geophysical Research: Oceans

RESEARCH ARTICLE
10.1029/2017JC013436

Seasonal and Interannual Mixed-Layer Heat Budget Variability in the Western Tropical Atlantic From Argo Floats (2007–2012)

A. V. Nogueira Neto[1,2], H. Giordani[1], G. Caniaux[1], and M. Araujo[2,3]

[1]Centre National de Recherches Météorologiques, CNRM-UMR3589 (Météo France/CNRS), Toulouse, France, [2]Laboratório de Oceanografia Física e Costeira, LOFEC-UFPE, Pernambuco, Brazil, [3]Brazilian Research Network on Global Climate Change—Rede CLIMA, São Paulo, Brazil

Key Points:
- A mixed-layer heat budget is performed in the western tropical Atlantic with Argo floats from 2007 to 2012, a relatively well sampled period
- Outside of the equator, the surface fluxes dominate and in the equatorial band, the oceanic dynamics contributes to the seasonal cycle of SST
- The warm (cold) SST anomalies in 2010 (2012) were generated by anomalous surface fluxes in the tropical Atlantic during the previous winter

Correspondence to:
A. V. Nogueira Neto,
antonio.vasconcelos@meteo.fr

Citation:
Nogueira Neto, A. V., Giordani, H., Caniaux, G., & Araujo, M. (2018). Seasonal and interannual mixed-layer heat budget variability in the western tropical Atlantic from Argo floats (2007–2012). *Journal of Geophysical Research: Oceans*, *123*, 5298–5322. https://doi.org/10.1029/2017JC013436

Received 7 SEP 2017
Accepted 14 MAY 2018
Accepted article online 25 MAY 2018
Published online 8 AUG 2018

Abstract Oceanic and atmospheric processes were investigated in order to explore the causes of seasonal and interannual variability of sea surface temperatures (SST) in the western tropical Atlantic (WTA; 20°S–20°N, 15°W–60°W). A mixed-layer (ML) heat budget was performed by using Argo profiles and supplementary data sets based on satellite and atmospheric products during the period 2007–2012. The WTA is divided into four boxes which represent the main temporal and spatial heterogeneities of this region. An analysis of error of each term pointed out that the mean net surface heat fluxes are systematically underestimated by 20 W m^{-2}. A correction of this term provides realistic estimates of the vertical mixing which was obtained as residual term. In agreement with previous studies, the results show that surface flux is the most important process that governs the seasonal cycle of the heat content. Changes in shortwave radiation and latent heat fluxes dictate the oceanic response to the meridional migration of the ITCZ. Along the equator, surface fluxes modulate the annual cycle of ML temperature, but are strongly balanced by horizontal advection. The entrainment term proves a small contribution to the cooling of the ML. On an interannual time scale, the strong positive (negative) SST anomalies observed in 2010 (2012) were generated during the previous winter in both years, mainly north of 10°N, during which the wind anomalies were at the origin of intense heat loss anomalies. Horizontal advection may contributes to the maintaining of these SST anomalies in the equatorial zone and south Atlantic.

1. Introduction

Seasonal SST changes in the tropical Atlantic reflect a combined effect of the antisymmetric seasonal cycle of shortwave radiation and latent heat flux between the hemispheres and seasonal changes in ocean circulations. The resulting air-sea interaction maintains a zonally oriented band of SSTs exceeding 27°C which is associated with the Inter Tropical Convergence Zone (ITCZ) position (Foltz et al., 2003; Hastenrath, 2012; Hounsou-gbo et al., 2015; Wagner, 1996). During boreal spring the ITCZ is in its southernmost position, near the equator, when the SST in the northern tropics drop due to a northeast trade intensification. In boreal summer, the southeast and cross-equatorial wind intensification lead to strong northward SST gradients in the eastern equatorial Atlantic. During this period, a minimum of SST is observed centered a few degrees south of the equator and extending to 20°W. This is known as the Atlantic cold tongue (ACT). The northward SST gradient observed during this season contributes to keeping the ITCZ north of 5°N.

SST patterns are also influenced by the seasonal cycle of surface currents, which also have an important role in interhemispheric heat transport. In this region, a complex system of equatorial currents and counter currents are described as a source of heat for the Atlantic western bordering and as part of the meridional overturning circulation (MOC) (Schott et al., 1995). The variability of the major surface currents reflects the oceanic dynamic response to changes in wind field and the displacement of ITCZ. During spring and summer the westward flow of the North Equatorial Current (NEC) and South Equatorial Current (SEC) also show a small shift northward without significant changes in velocity (Merle & Anoult, 1985; Stramma & Schott, 1999). In summer, changes in cross-equatorial winds in the central basin contribute to the intensification of the central branch of the SEC (cSEC), which feeds the strong northwestward flow of the North Brazilian Current (NBC) along the Amazon continental shelf break (Bourlès et al., 1999; Johns et al., 1998). In summer and fall, north of 8°N the NBC retroflects into the eastward flowing North Equatorial Counter-Current (NECC) (Stramma & Schott, 1999).

Superimposed on the seasonal cycle, two main climate modes are present in the tropical Atlantic. They are related to the SST variability in interannual to decadal time scales. One mode is related to the ocean zonal adjustment in the eastern equatorial Atlantic and to changes in trade winds in the central basin which is similar to El Niño in the equatorial Pacific. The other mode, first identified by Servain (1991) using principal component analysis, is characterized by an anomalous meridional SST gradient due to a north-south oscillation in SSTs. This mode is related to the mean position, the meridional displacement, and intensity of the ITCZ.

The knowledge of the main mechanisms responsible for the SST variability in the tropical Atlantic have contributed to a greater understanding of their impact on regional climates and/or extreme climatic events over the Northeast of Brazil, the Caribbean area, Sub-Saharan Africa, and the Angola coast (Caniaux et al., 2011; Hastenrath, 1984; Hastenrath & Greischar, 1993; Hounsou-gbo et al., 2015). Recent studies have reported climatic and oceanographic events which occurred during or between 2010 and 2012 as being linked to SST anomalies in the tropical Atlantic. The SST anomalies reached 1.5°C and −1.5°C in 2010 and 2012, respectively (Marengo et al., 2013; Sodré & Souza Filho, 2013). Such anomalies contributed to: extreme events of precipitation in the eastern coast of the Northeast of Brazil (166.8% above the norm in June 2010), high tropical cyclone activity (in 2010), changes in air-sea fluxes of CO_2 (in 2010), an intense drought in northeast Brazil in 2012 (reaching 5 mm d^{-1} below the climatology between April and May 2012) and bloom *Sargassum* algae in central tropical Atlantic (started in 2011) (Ibánhez et al., 2016; Lefèvre et al., 2013; Lim et al., 2016; Marengo & Bernasconi, 2015; Marengo et al., 2013; Wang & Hu, 2016).

The causes of SST variability are usually explained by analyzing the atmospheric and oceanic processes regulating the mixed-layer heat content. Several studies based on observations (Foltz et al., 2003, 2013; Hummels et al., 2014; Wade et al., 2011) or models (Cintra et al., 2015; Giordani et al., 2013; Peter et al., 2006; Yu et al., 2006) estimated the causes of the SST variability in different regions of the tropical Atlantic. Yu et al. (2006) compared four products in order to investigate the role of the surface heat fluxes on the SST variability in the tropical Atlantic. They divided the tropical Atlantic into two regimes: the first represented the zones where the changes in SST were governed by surface fluxes, located north of 10°N and south of 5°S, the second one an equatorial band between 10°N and 5°S characterized by strong contributions of the ocean dynamical processes.

Using measurements of mooring buoys from the PIRATA Project, Foltz et al. (2003, 2013) estimated the mixed-layer heat budget in the tropical Atlantic. They corroborated Yu et al. (2006) and showed that the annual cycle of the heat content in the mixed-layer, north of 8°N, is mainly driven by the shift of the warming phase by shortwave radiation and the cooling by latent heat loss. In the northeastern tropical Atlantic, south of 8°N, Foltz et al. (2013) demonstrated the semiannual cycle of the mixed-layer heat content. It is controlled by the semiannual cycle of the shortwave radiation and balanced by the turbulent mixing (related to changes in the trade winds, inducing shallower thermocline and thinner barrier layers) in boreal spring and by the latent heat flux in boreal summer.

Along the Equator many studies have identified the important contribution of the horizontal and vertical advections, vertical mixing, and entrainment as the principal mechanisms responsible for cooling which compensates warming by surface fluxes (Foltz et al., 2003; Giordani et al., 2013; Peter et al., 2006; Wade et al., 2011). Based on PIRATA buoys data along the equator, Foltz et al. (2003) have shown that the seasonal cycle of mixed-layer heat content in the western (38°W) and central (23°W) equatorial Atlantic results from significant contributions of the entrainment, zonal and eddy heat advections, caused by seasonal changes in the intensity of the SEC and the propagation of tropical instability waves (Foltz et al., 2003). In the east (at 10°W), vertical processes, namely entrainment and vertical diffusion, are major contributors to the strong seasonal cooling of SST. Wade et al. (2011) also investigated the heat budget based on Argo float profiles in the eastern equatorial Atlantic. They evidenced that vertical mixing was the second most important contributor to the annual cycle of the mixed-layer heat content, after surface fluxes.

Using a global ocean model, Peter et al. (2006) obtained a closed mixed-layer heat budget of the equatorial Atlantic and estimated the vertical terms that cannot be directly computed and evaluated from observational studies. Their results proved a great contribution of horizontal advection and entrainment in the equatorial Atlantic and the major role of vertical processes in the evolution and maintenance of the ACT during boreal summers. More recently, using a regional model in the ACT region, Giordani et al. (2013)

stressed the major role of vertical mixing and horizontal advection, both of which are controlled by the variability of wind energy flux.

As reviewed above, extensive studies were conducted in order to explore the causes and effects of the SST variability based on heat budget components in the tropical Atlantic. However, most of the observational studies were restricted to mooring buoys, as in Foltz et al. (2003, 2013), or to the eastern equatorial basin (Giordani et al., 2013; Wade et al., 2011). Some regions in the west and/or out of the Equatorial zone are not yet well documented therefore, at least in observational studies. For example, in the southwestern tropical Atlantic and in the oceanic region adjacent to the Amazon river mouth, few model studies have provided analyses concerning the most important contributors toward the evolution of the SSTs variability (Cintra et al., 2015; Servain & Lazar, 2010).

Observational studies are also limited in explicit evaluation of all oceanic processes contributing to SST changes. They provide even so, fundamental information to support model studies used as a complementary tool for the comprehension of tropical Atlantic SST variability. In this context, this study proposes a mixed-layer heat budget by using Argo float profiles and satellite-based products in the whole western tropical Atlantic (WTA, i.e., 20°N–20°S, 15°W–60°W) between 2007 and 2012. We intend to evaluate the causes of SST changes on seasonal and interannual time scales. We also intend to evaluate the Argo array representation on a regional scale.

The paper is structured as follows: section 2 describes the methodology and data set; section 3 illustrates the seasonal cycle of SST; the contribution of the heat budget terms is estimated and discussed in section 4; and finally, the main findings are summarized in section 5.

2. Materials and Methods

2.1. Data and Quality Check

To estimate the mixed-layer heat budget, we used hydrographic measurements and supplementary data such as SST reanalysis, horizontal currents, and surface flux fields from various sources (Table 1). The primary data set consists of temperature and salinity vertical profiles measured by Argo floats. The Argo project is an international collaboration that have provided a global array of profiling floats for the monitoring of the hydrographic parameters in the upper ocean. The Argo floats generally work in a 10 day cycle as follows: once launched into the ocean, a float starts a typical 10 day cycle which includes an initial descent to a programmed "drift depth" (usually a depth of 1,000 m) where the float drifts for approximately 9 days. It then dives down to a depth of 2,000 m and begins to rise profiling the water column recording temperature and salinity measurements. When it surfaces, the Argo float transmits its measurements to Global Data Assembly Centers (GDAC) after which, the float sinks and another cycle begins.

Four GDAC are responsible for making all Argo float data publically accessible after two levels of quality control (QC). The first one is the real-time QC that is an automatic set of quality tests on each parameter measured by the float. The second one is a delayed mode of QC performed by scientists in the data centers. For this study, we first downloaded 20,228 profiles from the Coriolis global data center (http://www.ifremer.fr//) available from 2000 to 2014 (Figure 1a). It includes both real-time and delayed mode profiles collected in the WTA.

Table 1
Data Set of Satellite-Derived Products Used to Estimate the Mixed-Layer Heat Budget

Data set	Parameters	Spatial resolution	Temporal resolution
OISST	Sea surface temperature	0.25°	Daily
ERA-Interim	Surface fluxes	0.25°	6 h
OSCAR	Surface currents	0.33°	5 day mean
GEKCO	Surface currents	0.25°	Daily

Note. For the computing of the mixed-layer heat budget the ERA-I surface fluxes, OSCAR, and GEKCO surface currents were interpolated on the OISST horizontal grid and at daily frequency.

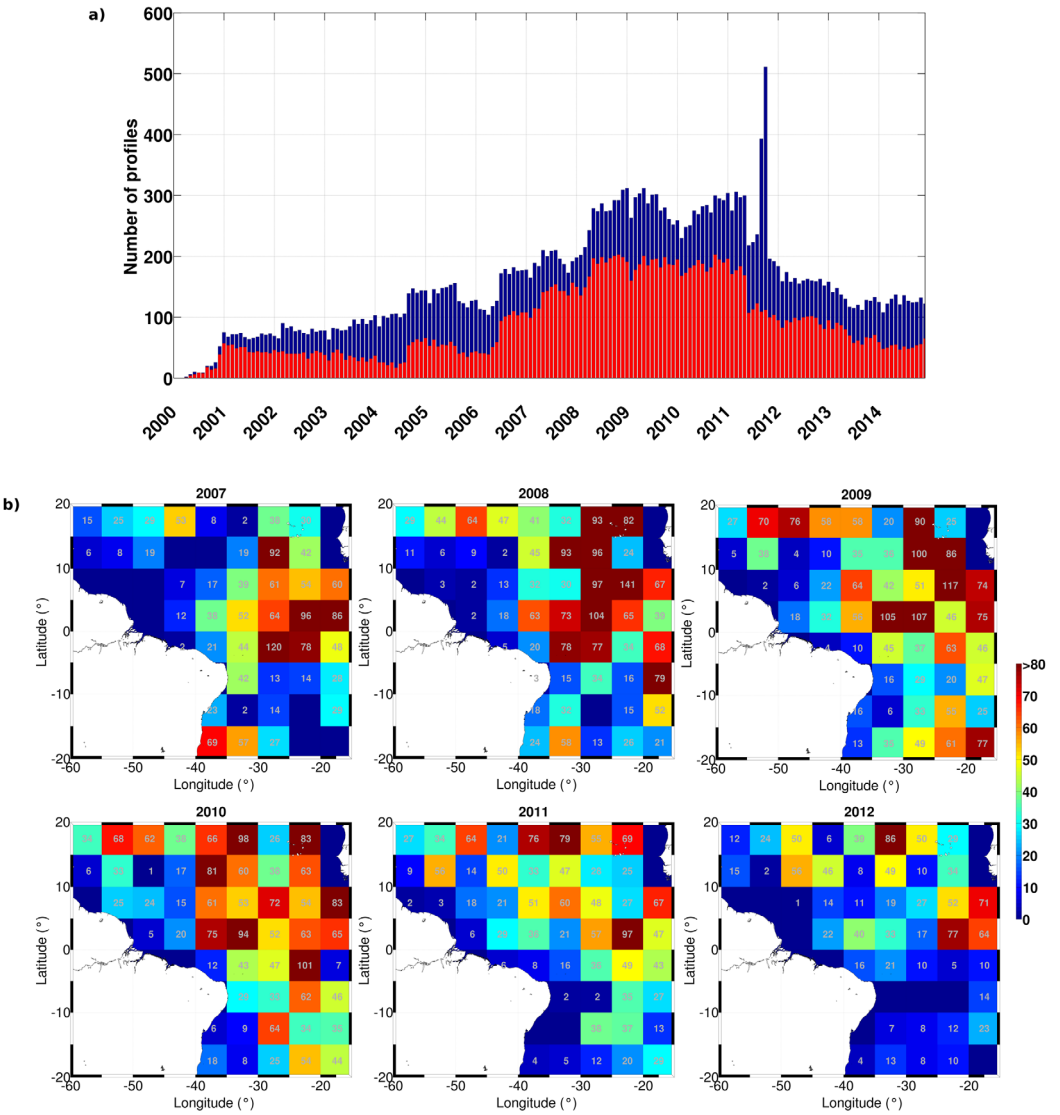

Figure 1. (a) Number of Argo float profiles from 2000 to 2014 (blue bars) and number of remained profiles after our quality control (red bars). (b) Number of Argo float profiles within 5° × 5° boxes for the years 2007–2012.

Answering the need for a high-quality and vertical regularly spaced data in the surface layer so as to estimate the mixed-layer depth (MLD) and to vertically integrate its temperature, we applied our own QC, based on Wade et al. (2011). At first, we used a low-pass filter to eliminate some spurious values. All profiles with more than five consecutive values flagged as bad values in the upper 300 m were eliminated. We then interpolated all profiles on a regular vertical grid of 5 m. After interpolation, the profiles that presented missing values in surface (5 m depth) were also eliminated. The QC procedure eliminated around 43% of the total Argo profiles downloaded (2000–2014).

To minimize the impacts of temporal and spatial gaps in Argo sampling and data gaps from QC procedure, we decided to use only the temperature and salinity profiles measured from 2007 to 2012, which represent the most sampled years since the Argo project started. Considering only this period, 17,537 profiles were measured in the WTA 37% of which were eliminated by our QC. Figure 1a shows the amount of initial (blue bars) and remaining profiles (red bars) after QC and the spatial distribution of the remained profiles in the study area for every year between 2007 and 2012 (Figure 1b). It is noteworthy that the number of profiles across the whole domain increases until 2010. A significantly decrease of profiles is observed from 2011 mainly in the south tropical Atlantic (5°S–20°S).

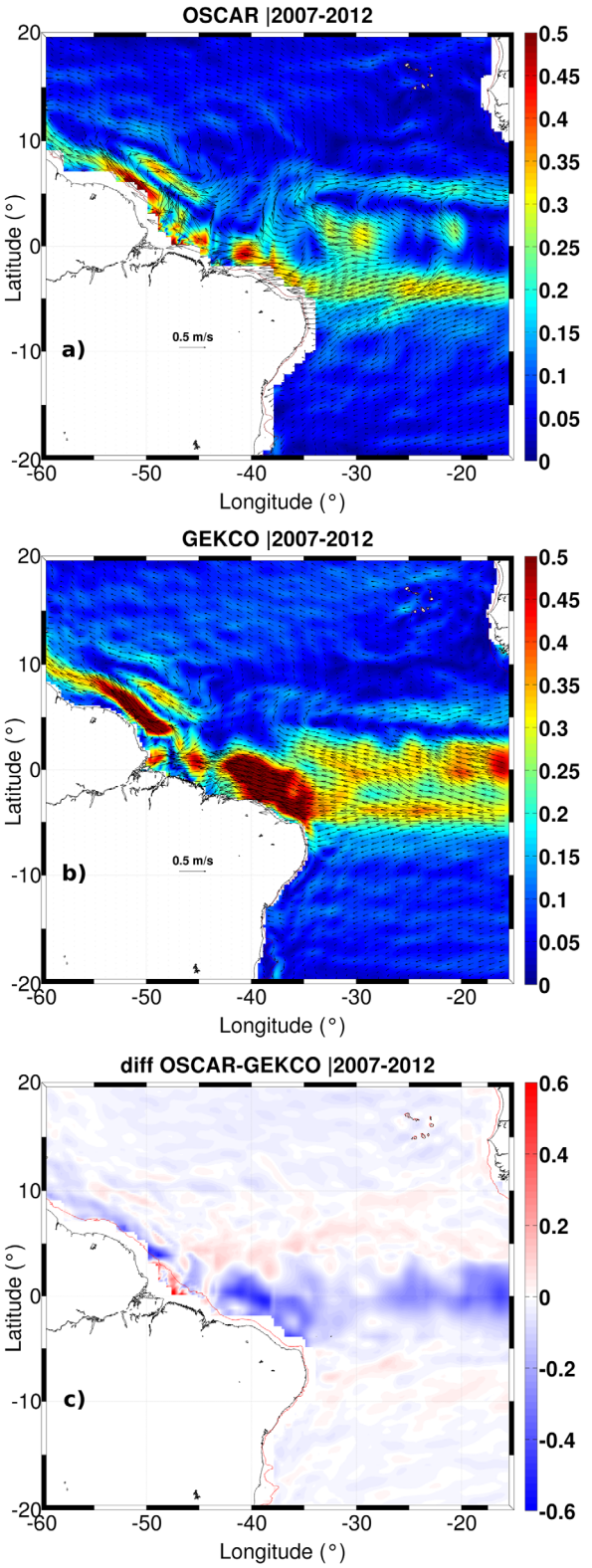

Figure 2. Comparison between mean (a) OSCAR and (b) GEKCO currents (arrows) during the 2007–2012 period. Current magnitude shaded (m s^{-1}). (c) Difference of magnitude of the currents OSCAR-GECKO during the same period.

As supplementary data, we used the daily SSTs obtained from NOAA Optimum Interpolation Sea Surface Temperatures (OISST) (Reynolds et al., 2007; hereafter SSTr) available on a regular 0.25° latitude × 0.25° longitude grid. This product includes satellite SST retrievals from Advanced Very High Resolution Radiometer (AVHRR—from 1981 to the present) and additional data from the Advanced Microwave Scanning Radiometer on the Earth Observing System (AMSR—from 2002 to 2011).

We decided to compare two products of surface currents in our estimations: the Ocean Surface Current Analysis Real-time (OSCAR) (Bonjean and Lagerloef, 2002) and the Geostrophic and Ekman Current Observatory (GEKCO), developed at the Laboratoire d'Etudes en Géophysique et Océanographie Spatiales (LEGOS), France (Sudre et al., 2013; Sudre & Marrow, 2008). Both products are based on satellite-derived measurements for the estimation of geostrophic and Ekman currents.

OSCAR products are available every 5 days on a 0.33° latitude × 0.33° longitude grid. The database used includes winds from scatterometer for estimation of the Ekman currents and Topex Poseidon/Jason 1 altimetry for geostrophic currents.

GEKCO provides daily mean currents on a global regular 0.25° latitude × 0.25° longitude grid. It uses the same database as OSCAR for Ekman currents. Geostrophic currents, however, were estimated by using SSH anomalies from the Data Unification and Altimeter Combination System (DUACS) product, which includes measurements from five satellite missions (Topex/Poseidon, Jason 1, ERS1&2, Geosat Follow-on, and Envisat) (Sudre & Morrow, 2008).

Johnson et al. (2007) compared OSCAR current estimates with drifters and shipboard ADCP data in the near-equatorial region. They indicated that OSCAR provides accurate estimates of zonal currents variability with correlations ranging from 0.5 to 0.8 for periods shorter than 40 days, but that this correlation decreases at latitudes higher than 10°. In the same way, comparisons of GEKCO current estimates with in situ data performed by Sudre et al. (2013) in tropical regions evidenced correlations around 0.7 for zonal currents. In general both products poorly reproduce the meridional component of the currents with correlations smaller (<0.5) than those observed for the zonal component.

Figure 2 compares the mean current field over the 2007–2012 period for both products. Higher current intensities of up to 0.4 m s^{-1} are observed along the equator and near the north Brazilian coast. GEKCO currents are about 0.4–0.5 m s^{-1} stronger than OSCAR currents mainly in the equatorial region and such differences are due to the temporal resolution of the products (daily for GEKCO and every 5 days for OSCAR). The differences can also be attributed to the treatment of the equatorial band where the Coriolis force vanishes creating a singularity in the usual geostrophic current formulation ($\frac{g}{f}k\wedge\nabla h$), where h is the dynamic topography). In the equatorial band, Jerlov (1953), Hidaha (1956), Moore and Philander (1976), and more recently Giordani and Caniaux (2011) suggest the use of the second derivative of the altimetry field for the estimation of the zonal component of the current ($\frac{g}{\beta}\nabla^2 h$). Further from the equator, the continuity between

these equations is ensured by applying a spline function within the 2°N–2°S band (Sudre et al., 2013). Differences between GEKCO and OSCAR currents come from the spline function and from the width of the connecting band. These differences are sources of uncertainties on horizontal advection estimates.

We also used daily averaged surface heat fluxes from the ERA-Interim reanalysis (Dee et al., 2011) of the European Center for Medium-Range Weather Forecasts (ECMWF). This data set comprises net shortwave and longwave radiation fluxes, latent and sensible heat fluxes on a regular spacing grid of 0.5° latitude × 0.5° longitude. This reanalysis is largely used as a surface fluxes database (e.g., OAFlux, TropFlux), which were found to well correlated to local estimations of surface fluxes (Caniaux et al., 2017).

All these supplementary data were linearly interpolated to match the spatial and temporal resolutions of the SSTr before computing horizontal advection and net surface fluxes needed to estimate the mixed-layer heat budget.

2.2. Formulation of the Mixed-Layer Heat Budget

The heat budget in the oceanic mixed layer represents the balance of various processes that contribute to the variability of the heat content in the upper ocean and, consequently, affect the seasonality of SSTs. In the present study, the mixed-layer heat budget was estimated in the same way as in previous studies on the tropical Atlantic (e.g., Giordani et al., 2013; Foltz et al., 2013; Wade et al., 2011), and is expressed as follows:

$$\underbrace{\rho_0 C_p h \frac{\partial T}{\partial t}}_{\text{heatstorage}} = \underbrace{F_{sol}(I_{-h} - I_0) + \mathrm{F}_{nsol}}_{\text{S.flux}} - \underbrace{\rho_0 C_p h \overline{U} \nabla T}_{\text{Hadv}} - \rho_0 C_p \underbrace{h\{T - T_{-h}\} W_{e(-h)} + RES}_{W_e} \quad (1)$$

In equation (1), h is the MLD; $\overline{X}$ represents the vertical average in the mixed layer; h, T, and U, the mixed-layer depth (MLD), the temperature, and horizontal currents, respectively.ρ_0 is the surface density calculated from the SST and SSS of the Argo floats and C_p is the heat capacity of the sea water (3,984 J kg^{-1} °C). F_{sol} is the incident net shortwave radiation; F_{nsol} represents the nonsolar flux, which is the sum of latent, sensible heat fluxes, and the net longwave radiation. S.flux term in equation (1) takes into account the difference between the fraction of solar radiation that reaches the sea surface (I_0) and the fraction that penetrates down to the base of the mixed layer (I_{-h}).

The left-hand side term of equation (1) (heat storage) represents the temporal evolution of the mixed-layer temperature. It is expressed in terms of the net surface heat flux (S.flux), horizontal advection (Hadv), entrainment at the base of the mixed layer (W_e), and a residual term (RES). The residual term includes accumulated errors which affect all other terms of the heat budget in equation (1) and processes which cannot be explicitly estimated from observed data. However, as in Foltz et al. (2003) and Wade et al. (2011), the RES term may be representative of the turbulent mixing at the base of the mixed layer ($wT_{(-h)}$). Only the horizontal diffusion was omitted in equation (1) because this term was expected to be at least one order of magnitude smaller than the other terms at basin and boxes scales. At this spatial scales, the coefficient of horizontal diffusion is probably very small because of weak horizontal thermal and dynamical gradients, this is due to large Rossby radii of deformation at these latitudes and the spatiotemporal scales of Argo floats (Wade et al., 2011).

The heat storage was calculated by using a finite centered difference scheme, i.e., at the mean time and position between two consecutive Argo profiles. We considered a minimum time step dt of 10 days (one Argo cycling time) and a maximum of 30 days between two profiles (in case of missing or QC rejected profile). If the time period during two profiles exceeds 30 days, the budget is not calculated because this period is thought to be too large to produce representative budgets. At each profile position, a mixed-layer temperature was computed over depth h (the method used is described in the next subsection). The difference of mixed-layer temperatures between two successive positions of the float was then evaluated and multiplied by the mean MLD in order to obtain the heat storage term in equation (1).

To estimate the H.adv term, the daily mean SSTr field and both the OSCAR and GEKCO currents were used (these two current products were used to provide an error estimate in the budgets). It was assumed, as in Wade et al. (2011), that SSTs and surface currents are similar to the vertically averaged temperature $\overline{T}$ and horizontal current $\overline{U}$ in the mixed layer, i.e., these two quantities are supposed to be uniform across the MLD.

The entrainment velocity W_e is expressed as:

$$W_{e(-h)} = W_h + \partial_t h + \overline{U}\nabla h \quad (2)$$

where W_h is the vertical velocity (Ekman pumping) at the base of the mixed layer, $\partial_t h$ is the local tendency of h and $\overline{U}\nabla h$ is the lateral induction, which were estimated by using monthly MLD climatology fields calculated from Argo profiles. These fields were obtained by optimal interpolation of individual Argo MLDs onto a 0.25° longitude and 0.25° latitude grid following the procedure of De Mey and Ménard (1989). At each grid point, an initial MLD field (the guess) was corrected with all Argo MLDs calculated for the same month of the period 2000–2014. These lie within one influence time/space radius around the grid point. An isotropic space correlation radius of 700 km, and a decay *e*-folding time of 30 days was chosen after several sensitivity tests. The initial guess was homogeneous and taken at 60 m. The next month analysis then used the previous month analysis as a new guess.

The horizontal current was expressed as monthly climatology so as to compute the $\overline{U}\nabla h$ term in equation (2).

During one time step *dt*, a mean S.flux, Hadv was calculated from daily fields (monthly for W_e because it depends on the $\overline{U}\nabla h$). The mean fields were then linearly interpolated to the mean daily positions of the Argo float between two consecutive profiles (time step). In this way, all the terms of equation (1) are located at the same position and collocated in time.

2.3. Mixed-Layer Depth (MLD)

The MLD was calculated from each Argo profile by using the split-and-merge (SM) method (Thomson & Fine, 2003). This method consists of decomposing the profile into different segments by splitting the initial fitted curve at break points of the available data. Each segment represents an approximation by a first-order polynomial in which the difference with respect to the observed curve (error norm) does not exceed a given predefined threshold chosen by the user. The segments with similar approximating coefficients are merged and the MLD is defined at the base of the first segment (the first break point).

According to Thomson and Fine (2003), the SM method gives almost the same results as the threshold method based on a given density criterion, but is less sensitive to changes in the error norm than conventional methods seems to be. We confirm their conclusions after comparing numerous MLDs estimated from density profiles and computed from the SM method and classical density criterion (de Boyer Montégut et al., 2004) at each Argo profile over the WTA. To evaluate the methods, we chose an error norm/threshold of 0.02 and 0.03 (kg m^{-3}, for the density criterion), within the range of values used in Thomson and Fine (2003) and de Boyer Montégut et al. (2004). To compare the MLD estimated by these two methods, an ANOVA was performed with a sample of 100 profiles taken randomly in different regions of the WTA. The MLD from both methods and between the two values of error norm/threshold was tested. The result showed that both methods and error norm/thresholds were similar ($p > 0.05$). Tukey's test was used to determine the normality and Barllet's test was used to determine the homogeneity of the variances.

Additionally, visual inspections of the profiles were performed to check the results when the difference between the two methods was larger than 10 m for a given profile. In most of the cases, the SM method displays better MLD estimates using an error norm of 0.02. Finally, we decided to retain an error norm of 0.02 to estimate the MLD at each Argo profile in this study. As in previous studies, which estimated mean seasonal and/or climatological MLD variability (e.g., Araujo et al., 2011; de Boyer Montégut et al., 2004; Vauclair & du Penhoat, 2001), this value is assumed to be representative of the mean MLD estimates using density profiles.

2.4. Regional Heterogeneities

The mixed-layer heat budget is presented in four boxes which reflect the main regional heterogeneities of the WTA (Figure 3). The boxes were delimited taking into consideration (i) the standard deviation of the mean SST; (ii) the mean net surface heat flux; and (iii) the mean distribution of zonal currents. Additionally we try to encompass all regions where the heat budget terms were estimated in previous studies (Foltz et al., 2003, 2013; Giordani et al., 2013; Wade et al., 2011; Yu et al., 2006).

Boxes 1 and 2 are located north of the WTA. Box 1 is a northwestern zone between 10°N and 20°N, west of 35°W. The northeastern tropical Atlantic is represented in box 2, located east of 35°W, between 10°N and 20°N. It includes the northern part of the region considered in Foltz et al. (2013). The northern tropical Atlantic is under the influence of the northeasterly winds as well as the NEC (box 1) and the NECC. Note that the

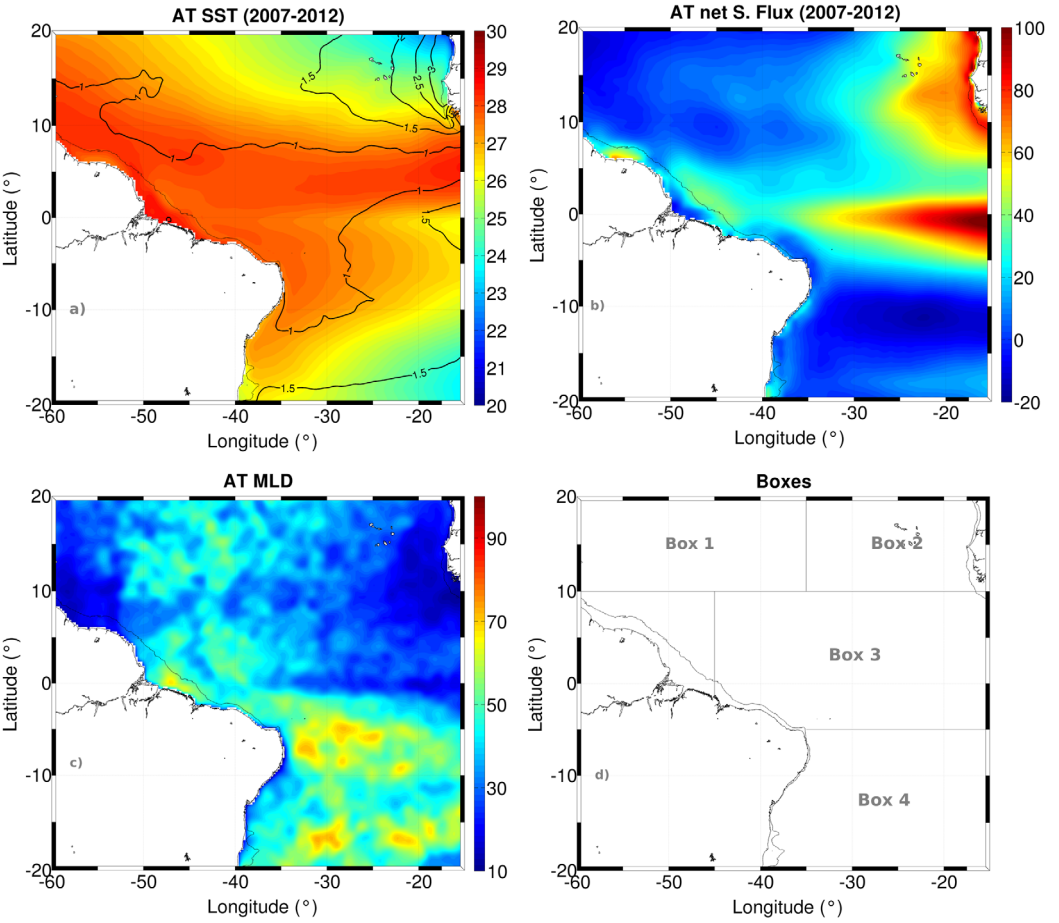

Figure 3. General mean field of the main parameters considered to describe the regional heterogeneities of the WTA. (a) SST (contours indicate the standard deviation), (b) net surface heat flux, (c) MLD obtained from Argo floats, and (d) the four regions chosen to describe the SST variability and the mixed-layer heat budget. Northern tropical Atlantic (boxes 1 and 2), western equatorial Atlantic (box 3), and south tropical Atlantic (box 4).

SST variability in box 2 is higher than in box 1 (Figure 3), partly due to important horizontal SST gradients: this led us to distinguish the difference between the two boxes.

The dynamical singularities of the equatorial zone, as discussed in Peter et al. (2006) and Giordani et al. (2013), were considered for box 3. They concern the zone between 5°S and 10°N; 45°W and 15°W and they represent a zone of weaker SST variability, under the influence of the strong western boundary and equatorial currents. Within this box equatorial dynamics are predominant. In addition, a pronounced SST gradient is observed in a boreal summer and fall, related to the latitudinal displacement of the ITCZ and ACT development (Foltz et al., 2013; Giordani et al., 2013).

Finally, box 4 is located south of 5°S. In this zone, higher temperatures are observed in the western region as well as deep mixed layers throughout the year (Cintra et al., 2015). The seasonal variability of surface heat fluxes influenced by the southeasterly trade winds is reversed in comparison with the northern regions (boxes 1 and 2; Figure 3). This region is also under the influence of the southern branch of the westward flowing SEC responsible for transporting south Atlantic surface water to the equatorial region and then on to the north hemisphere by the NBC (Stramma & Schott, 1999).

3. Regional and Seasonal Variability of SSTs

In this section, we describe the mean seasonal evolution of SST in each box based on Argo data, and discuss how the sampling and spatial distribution of Argo profiles may influence the seasonal representation of SST and the heat budget estimates. To this end, we compare the mean seasonal cycle of the monthly gridded

SSTr averaged over a given box, the monthly SSTr collocated at the same position as the Argo profiles ($SSTr_{Argo}$) and the monthly mean mixed-layer temperature $\overline{T}$ obtained from Argo profiles, considered to be representative of the SST estimate (Figure 4).

In box 1, the minimum of SST, approximately 25.4°C, is observed in February. It increases during late spring and summer and reaches its maximum temperature (28.2°C) in October. The minimum of $\overline{T}$ is observed in March (Table 2). In general, $\overline{T}$ and $SSTr_{Argo}$ seasonal cycles are slightly underestimated compared with those of the SSTr, but they display a high correlation coefficient of 0.9. The almost constant number of profiles considered in the means (around 150 profiles/month, Figure 4) and their spatial distribution do not significantly influence the representation of the SST annual cycle in this zone.

In box 2, the minimum SST for the three series ranges from 22.9°C to 24.09°C, and is reached in February–March. After this, SSTs increase to a maximum of 27.5°C in October (Figure 4). In this region, the standard error of the three series indicates a great variability (>1.6°C) in the first 5 months of the year (i.e., during the cold period). A large difference between averaged gridded SSTr and $\overline{T}$ or $SSTr_{Argo}$ is however observed during this period (up to 1°C). Despite a good correlation coefficient between the box-averaged SSTr with $\overline{T}$

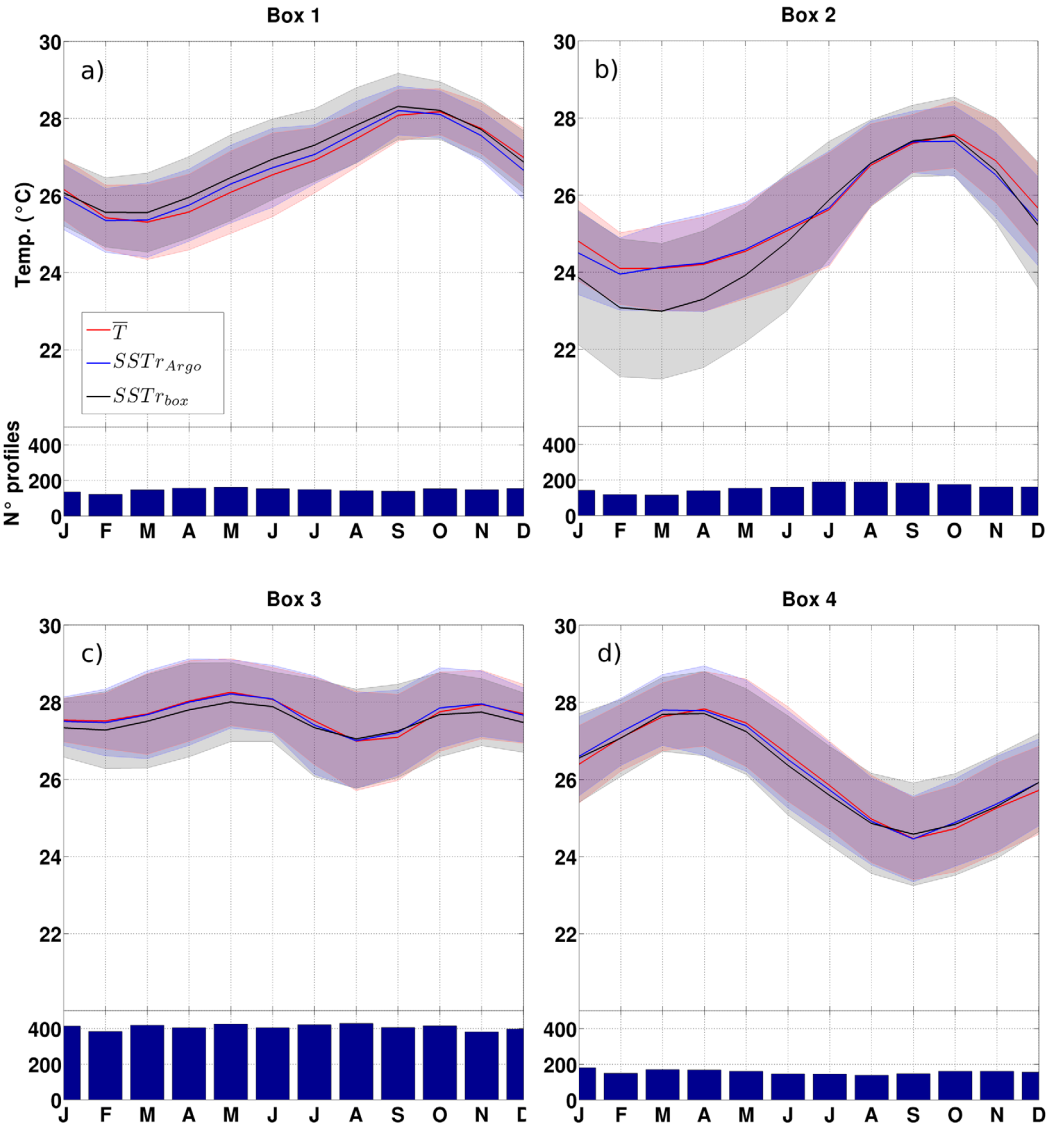

Figure 4. Seasonal cycles of $\overline{T}$ (red curve), $SSTr_{argo}$ (blue curve), and SSTr (black curve) during the period 2007–2012 for the five zones (temperature scale on the left in °C). Standard errors are indicated by shaded colors. The number of profiles per box is also indicated with blue bars.

Table 2
Main Characteristics of the Seasonal Cycles of the SST_r, SST_{argo}, and $\overline{T}$ Series in Each Box With Minimum, Maximum Values and Months, and Range of the Seasonal Cycle (°C)

Box	Series	Min./Month	Max./Month	Range
1	SST_r	25.56/February	28.31/September	2.75
	SST_{argo}	25.35/February	28.2/September	2.85
	$\overline{T}$	25.31/March	28.18/October	2.87
2	SST_r	22.9/March	27.5/October	4,51
	SST_{argo}	23.95/February	27.4/October	3.45
	$\overline{T}$	24.09/February	27.57/October	3,48
3	SST_r	27.05/August	28/May	0,95
	SST_{argo}	27/August	28.21/May	1.21
	$\overline{T}$	26.99/August	28.25/May	1.26
4	SST_r	24.58/September	27.7/April	3.12
	SST_{argo}	24.46/September	27.8/March	3.34
	$\overline{T}$	24.46/September	27.83/April	3.36

(0.98) and $SSTr_{Argo}$ (0.97), the seasonal cycle of $\overline{T}$ and $SSTr_{Argo}$ do not match that of the SSTr. The number of profiles during the period is always superior to 100 profiles/month and we attribute this large difference in boreal winters and springs to the limited spatial distribution of profiles (Figure 1). Argo floats do not sufficiently cover the northwestern African coast meaning that the cold waters associated with the upwelling present in this region are under sampled. This also means that SSTs in the upwelling region make an important contribution to the amplitude of the mean seasonal cycle and to the interannual variability in box 2.

In box 3, high SST values (>27°C) are observed yearlong with a good correlation between the three series (>0.95). The annual cycle of SST presents a semiannual signal with a weaker minimum in February and a stronger minimum in August (∼27.01°C). Maximums are observed in May (∼28.15°C) and November (∼27.8°C). In box 3, the Argo sampling is around 400 profiles per month which allows good spatial coverage (Figure 4). The relatively high amount of profiles in this zone can be explained by the presence of strong zonal currents such as the NBC, with 1 m/s in the first 100 m, and its retroflection into the NECC and the EUC (Bourlès et al., 1999; Johns et al., 1998; Nogueira Neto & Silva, 2014). These currents contribute to the rapid spread of the profilers a distance from the north Brazilian coast and they maintain the Argo floats in the central basin. It is interesting to observe that during boreal summer the SST cooling is delayed by about 1 month with respect to the maximum cooling period of the ACT, in the eastern equatorial Atlantic (Caniaux et al., 2011; Marin et al., 2009). The southern part of this box can thus be considered as a western extension of the ACT.

In box 4, a large amplitude of SST is again observed, as in the two northern boxes (Figure 4 and Table 2). The maximum temperature of the seasonal cycle is reached during the boreal spring at around 27.8°C (April–March) and the minimum at around 24.5°C in September. Box 4 is the largest zone considered in this study, but the number of Argo profiles per month for the period considered is similar to box 1 (approximately 150 profiles/month). To conclude, the set of profiles between 2007 and 2012 has good spatial distribution and the Argo sampling can be considered representative of at least the mean seasonal cycle of SST in this area. The correlation coefficient of 0.9 among the three series and amplitudes confirms this.

4. Mean MLD Heat Budget in WTA

The SST variability reflects the balance among the principal oceanic and atmospheric processes on different temporal and spatial scales. To examine the relative contribution of the high-hand side terms of equation (1) to the heat storage, we hereby present a discussion based on the mean of each term in each box.

In the work of Foltz et al. (2003) and Wade et al. (2011), the residual term (which closes the heat budget) is used to estimate the vertical mixing contribution to the heat budget but it is associated with an analysis of error of the heat budget components in order to estimate the degrees of confidence that one can have on this processes in each box. This analysis sets the limits of the method and allows one to derive the vertical mixing and its reliability, i.e., an advanced process from observation data only.

Table 3
Mean Values of the Different Terms of the Budget Each Box (W m^{-2})

Box	Term	Value (OSCAR/GEKCO)
1	Heat storage	−5.7
	S.flux	−21.2
	H. advection	+0.64/+1.65
	Entrainment	−3.6/−3.8
	Residual	+18.6/+17.7
2	Heat storage	−7
	S.flux	+3.8
	H. advection	−0.89/−2.1
	Entrainment	−9.02/−9.42
	Residual	+1.08/+0.53
3	Heat storage	−1.07
	S.flux	9.94
	H. advection	−9.3/−10.05
	Entrainment	−5.8/−6.14
	Residual	+4/+5.20
4	Heat storage	−15.6
	S.flux	−14
	H. advection	−2.8/−6.4
	Entrainment	−8.6/−8.7
	Residual	+10.3/+14.06

4.1. Relative Contribution of the Main Processes

According to Table 3, the year-mean net surface heat flux is the leading term heat storage in boxes 1, 2, and 5 which are located off the equatorial band. Box 3 is under influence of the SEC and the NEC. Consequently, the SST variability in both these boxes is mainly controlled by the circulation, namely the Hadv term, and surface net heat flux. Regarding the sign, the annual mean of the net surface heat flux (Table 3) is in good agreement with the patterns of NCEP and ERA-40 products in the Tropical Atlantic (see Figures 2c and 2d from Yu et al. (2006)). The absolute values of this term in all boxes however are always lower than those showed in Yu et al. (2006). This underestimation has a great impact on the residual term and closure of mixed-layer heat budget. This point will be discussed in the next section with a focus on the consequences on the residual term.

In box 1, the mean Hadv warms the mixed-layer while it induces a cooling in other regions. In box 3, Hadv reaches 10 W m^{-2}, which is a contribution similar to the net surface heat flux. In other boxes, this term ranges from 0.6 to 9.3 W m^{-2} (absolute value). The W_e term is negative everywhere signifying cooling up to 9.6 W m^{-2} in box 2 and 3.8 W m^{-2} in box 1.

As discussed in section 2.2, the closure term RES was estimated from the difference between the heat storage and the sum of right-hand side terms of equation (1). The year-mean RES is positive in all boxes reaching 18 W m^{-2} in box 1 (Table 3), Consequently, we conclude that RES cannot be assimilated to the vertical mixing term because it is necessarily negative according to the thermal stratification in the tropics. In fact, errors of each heat budget component accumulate and overshadow the physical signal (vertical mixing) contained in RES.

Investigating these errors can give extra information about the reliability and/or limitations in the data set and consequently the opportunity to extract physical information from the residual RES. For this reason, the following section presents an analysis of errors of each term of the heat budget in order to propose corrections which can lead, under specific contexts, to physical interpretations of RES.

4.1.1. Errors of the Heat Budget Components

The error analysis presented in this section is adapted from previous studies as Foltz et al. (2003) and Wade et al. (2011). Errors of the heat budget components were estimated from the total derivative expression:

$$\Delta f \approx \frac{\partial f}{\partial x_1}\Delta x_1 + \frac{\partial f}{\partial x_2}\Delta x_2 + \frac{\partial f}{\partial x_3}\Delta x_3 \ldots + \frac{\partial f}{\partial x_i}\Delta x_i \tag{3}$$

In equation (3), f represents the annual mean of a given term of the heat budget in a given box, x_i a parameter which represents a source of error in f and Δx_i is the error related to such parameter, which was based mainly on mean instrumental errors (or mean standard errors) shown in Table 4. The product of the sensitivity of f with respect to the parameters x_i and the increment Δx_i represents an uncertainty.

Table 4
Main Increment ∇x_i Used to Estimate Errors in Each Heat Budget Components

Parameter	Error
Air temperature (°C)	0.2
SST (°C)	0.003
Relative humidity (%)	0.02
Wind (m s^{-1})	0.3
U current (m s^{-1})	0.001
V current (m s^{-1})	0.001
MLD (m)	0.5
Cd	0.1×10^{-3}

Finally, an upper bound of the error which affects a function f is estimated by summing the squared of uncertainties

$$ER = \overline{\sum_i \left(\frac{\partial f}{\partial x_i}\Delta x_i\right)^2} \tag{4}$$

Following equations (3) and (4), the error affecting each component of the heat budget was estimated and shown in Table 5. Inspection of these errors shows that the primary and systematic source of error is around 20 W m^{-2} and affects the net surface heat flux in all boxes. Error estimates of Hadv and W_e are weak, under 3 W m^{-2} and do not present a great difference when using OSCAR and GEKCO currents. Error affecting the heat storage is weak except in box 4 where they

Table 5
Mean Errors on the Different Terms of the Budget Each Box (W m^{-2})

Box	Term	Error (OSCAR/GEKCO)
1	Heat storage	4.39
	S.flux	24.22
	Latent heat flux	22.43
	Sensible heat flux	1.36
	Fsol	4.54
	H. advection	1.56/2.16
	Entrainment	1.89/1.92
	Residual	25.15/25.2
2	Heat storage	7.18
	S.flux	20.46
	Latent heat flux	18.35
	Sensible heat flux	1.29
	Fsol	4.64
	H. advection	0.9/1.29
	Entrainment	2.05/2.15
	Residual	22.29/22.35
3	Heat storage	8.62
	S.flux	20.17
	Latent heat flux	17.95
	Sensible heat flux	1.31
	Fsol	4.31
	H. advection	1.0/2.5
	Entrainment	1.65/2.12
	Residual	22.44/22.61
4	Heat storage	16.84
	S.flux	22.96
	Latent heat flux	21.06
	Sensible heat flux	1.51
	Fsol	4.69
	H. advection	2.59/2.73
	Entrainment	2.83/2.85
	Residual	29.12/29.13

Note. The main error of the net surface flux term is also shown.

reach 16 W m^{-2} probably due to a poor Argo sampling. As the error estimate of the residual term is calculated by taking the square root of the sum of the squared error of each term (equation (3)), the residual error appears to be driven mainly by the net surface heat flux error and locally by the heat storage error (e.g., box 4). Unlike other components, error of the net surface heat flux is stable around 20 W m^{-2} in all regions which leads us to consider this error as a bias.

The stability of the net heat flux error is a good indication of the robustness and reliability of the bias affecting this forcing. A qualitative comparison between mean net surface heat flux from four products presented in Yu et al. (2006) highlights a bias larger than 20 W m^{-2}. Other previous studies such as Sun et al. (2003) and Yu et al. (2004); Klinker (1998) and Ayina and Bentamy (2006) have also evidenced that ECWMF net surface heat loss is overestimated by 29 W m^{-2} in the Tropical Atlantic at PIRATA buoys. This bias ranges between 20 and 80 W m^{-2} in the tropical Pacific and Indian Ocean. All authors also show that the latent heat loss is the main contribution to this bias and their results confirm our errors in the estimates shown in Table 5.

4.1.2. Correction in Net Surface Heat Flux and Residual Term

The residual term is an attempt to capture the turbulent mixing at the mixed-layer base. In this respect, it plays an important role in the mixed-layer heat budget as shown by Foltz et al. (2003) and Wade et al. (2011) in the Gulf of Guinea. The thermocline being stably stratified, the turbulent mixing always entrains cold water from the thermocline into the mixed layer must therefore always be negative or null to be considered as representative of the turbulent mixing.

The approach proposed is to correct the net surface heat flux from its bias in order to provide a new residual in each box. Certainly all errors such as the heat storage errors also affect the RES, especially in box 4, but not systematically which is why they were not used in the corrections. This approach based on corrections of the net surface heat flux is critical for the deriving of realistic vertical mixing but these corrections are systematically confirmed by previous studies mentioned above.

The corrected S.flux is positive in the whole domain (Figure 5), which means that the ocean gains heat by surface flux in annual mean. The highest values of S.flux are observed in the equatorial region (box 3) in the core of the ITCZ, and in box 2, a region under influence of strong wind variability. Mean S.flux decreases toward the poles, as observed in boxes 1 and 4. These patterns are comparable to other year-mean surface flux products (Yu et al., 2006). This result confirms once more that ECMWF products underestimate the net surface heat flux by 20 W m^{-2} in average. It gives strength to our error estimate.

The mean new RES obtained after corrections is negative everywhere with physical order of magnitude (Figure 5). It presents high values in the equatorial and the northeastern tropical Atlantic (boxes 2 and 3) around −20 W m^{-2} while in other regions it is under −15 W m^{-2}. Vertical mixing was also estimated directly from 16,122 Argo profiles between 2007 and 2014 by using a K-profile parameterization. Time-averaged estimates display maximum cooling of −17 W m^{-2} around 45 m depth (Figure 6). These values are relatively close to the year-mean corrected RES and MLD (−13 W m^{-2} and 36 m depth, respectively) on a basin scale which gives confidence to the method used for the calculation of RES. The standard deviation of the vertical turbulent mixing exhibits a large variability (50 W m^{-2}) which points out the intermittent characteristic and the great spatiotemporal variability of turbulence. This independent estimation confirms the physical meaning of the corrected residual.

Additionally, based on dynamic conditions, the significant contribution of the RES found in boxes 2 and 3 is in agreement with the turbulent mixing expected for this regions. In box 3, turbulent mixing is attributed to the presence of the NECC and SEC, because these currents have the capacity to produce high mechanical

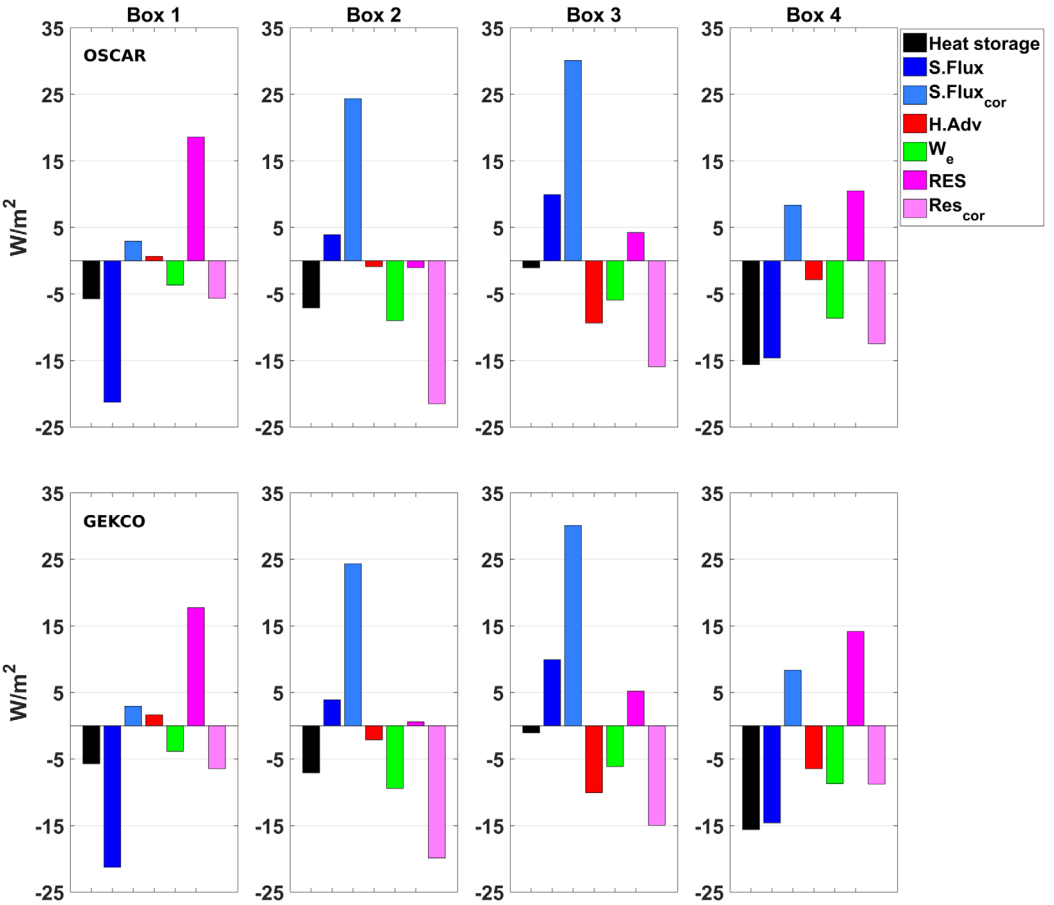

Figure 5. Relative contributions (in W m^{-2}) of the various terms on the right-hand side of equation (1) obtained with advection and entrainment computed from OSCAR and GEKCO currents. Corrected S.Flux and RES are shown.

production of turbulent kinetic energy from vertical shear. Box 2 (region north of 15°N) is not located in a region of current systems and the turbulent mixing draws its energy from the trade winds. We conclude then that the new corrected RES can be considered as representative of the vertical mixing, but under specific conditions explained by the regional dynamic context.

As explained previously, Hadv and W_e were not corrected. After correction of the S.flux term, heating by Hadv (from GEKCO) in box 1, however, presents almost the same contribution as S.flux (<3 W m^{-2}), while in box 3, it becomes weaker than S.flux (Figure 5). In boxes 2, 3, and 4, Hadv is negative, but after correction, it contributes to the balancing of S.flux in box 3, where equatorial currents are intense. The induced-cooling is always lower than 10 W m^{-2}, but associated with negative residual it contributes to the balancing of the surface flux heating in all regions (Figure 5).

4.2. Mean Seasonal Mixed-Layer Heat Budget

This section describes the mean seasonal cycle of the heat budget considering the corrected components (Figures 7–11). In all boxes, the heat storage is primarily controlled by the net surface heat flux while the other terms tend to balance it, except for box 4. Horizontal advections estimated from the OSCAR and GEKCO currents are consistent but differ in strong currents systems, namely in equatorial box 3, where the calculated correlation between them is 0.84. The residual term is discussed separately to evaluate whether the corrections performed in the previous section are reliable on a seasonal time scale.

4.2.1. Northern Tropical Atlantic (Boxes 1 and 2)

In boxes 1 and 2 (Figures 7 and 8), the mixed-layer tends to warm from March to September with a maximum of 27.9 W m^{-2} in May in box 1 and 28.6 W m^{-2} in June in box 2. The cooling period occurs during November–February with a maximum heat loss in January (69.5 and 61.8 W m^{-2}, respectively). The surface

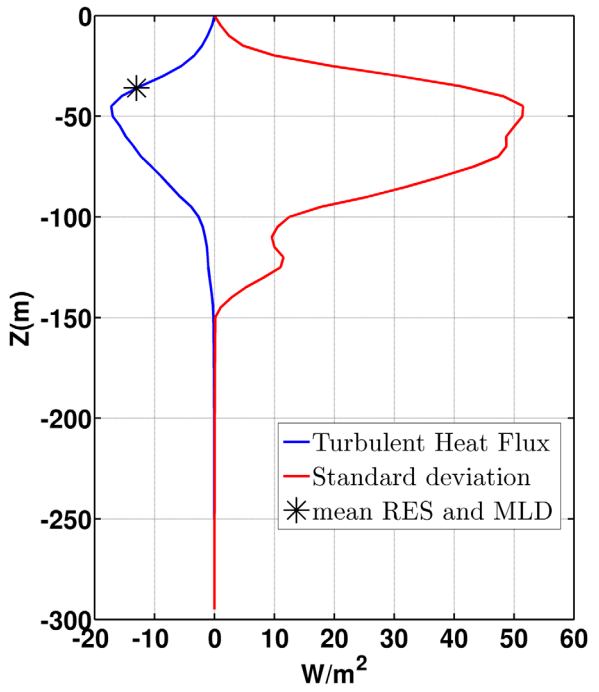

Figure 6. Mean vertical turbulent mixing (blue) and standard deviation (red) obtained from Argo profiles in the WTA during 2007–2012. The star indicates the magnitude of the residual term at the mean observed MLD.

flux is the most important term of the heat storage seasonal cycle over this region. The warming period is mainly explained by the prevalence of heat gain by shortwave radiation which is maximal in April–July, associated with a decrease of the latent heat loss due to a weakening of the northeasterly trade wind intensity from July to August. This occurs until the ITCZ has reached its northernmost position.

The heat storage variability is balanced by secondary, but quite important contributions of the oceanic dynamics. In box 1, the horizontal advection is close to zero during the warm period, but presents a weak positive contribution from November to February, also observed in box 2, probably due to Ekman divergence associated to intensification of zonal winds. It leads to a meridional advection of warm equatorial waters into this box (Figure 7). Our results in this region are comparable to those found by Foltz et al. (2003) at two PIRATA moorings located at 12°N and 15°N, along 38°W (box 1) and by Foltz et al. (2013) at PIRATA moorings in the northeastern tropical Atlantic, along 10°W. We find similar seasonal cycles, but with weaker amplitudes. These authors found imbalance between the heat storage and surface fluxes during a boreal fall and spring which were attributed to uncertainties in the latent heat flux. In this study, error estimates on each term of the mixed-layer heat budget (Table 5) have shown that the main uncertainty comes from the net surface heat flux and particularly from the latent heat flux, which is consistent with the findings of Foltz et al. (2013).

4.2.2. Western Equatorial Atlantic (Box 3)

In the equatorial box (Figure 9), the heat storage displays certain differences with respect to the other boxes in terms of range and annual cycles. Estimates of the heat storage in box 3 present a semiannual cycle modulated by surface heat fluxes. Two warming periods occur in

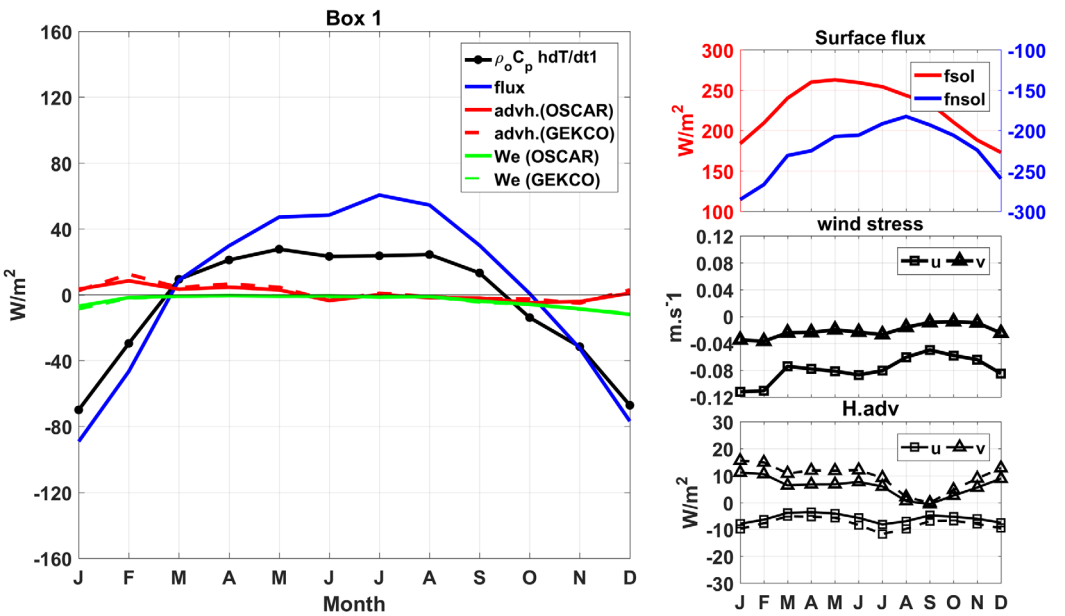

Figure 7. Heat budget terms of equation (1) in box 1 (heat storage in black, surface fluxes in blue, horizontal advection in red, entrainment in green, and horizontal advection and entrainment with OSCAR product in full line and dash with GEKCO). Top right figure shows the monthly mean shortwave radiation (red) and latent heat flux (blue); the middle right figure is the meridional (triangle) and zonal (square) components of the wind stress and in the bottom right figure the zonal (square) and meridional advection (triangle).

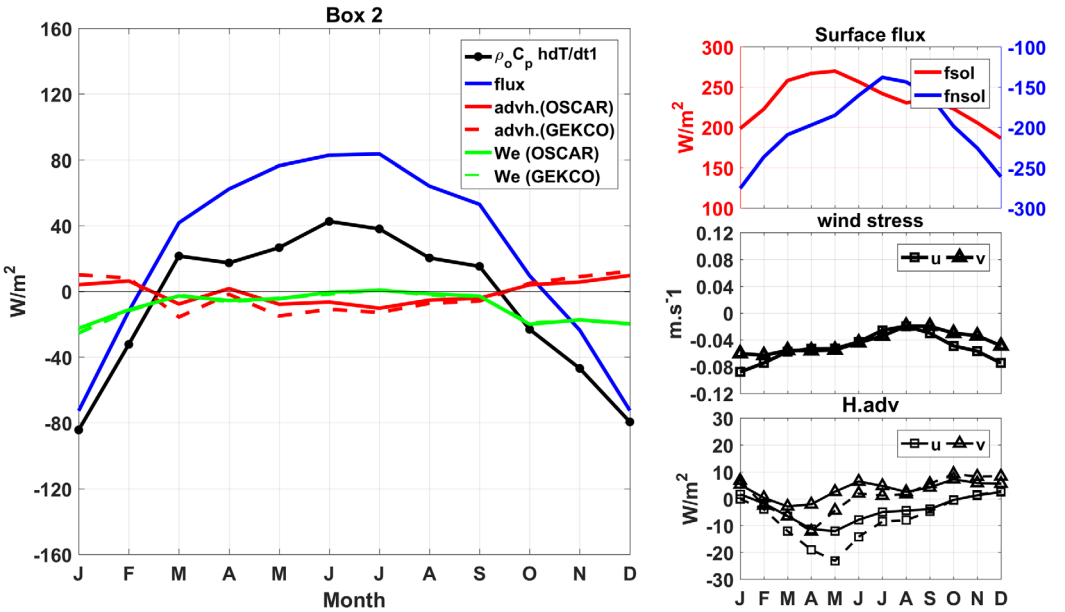

Figure 8. Same as Figure 7, but for box 2.

March–April (∼45 W m^{-2}) and September–October (∼20 W m^{-2}), which follow the semiannual cycle of the shortwave radiation (Figure 9).

Between these warm periods, two relatively cooling periods are observed during which the oceanic processes contribute largely to the SST tendencies (Figure 9). During the first (July–August), the heating by net surface flux decreases to around 12 W m^{-2} as a result of a decrease in shortwave radiation combined with an increase in cooling by latent heat flux. A weak positive horizontal advection (10 W m^{-2}) warms the surface layer (Hadv from GEKCO) and is partially compensated by an increase in cooling by entrainment. The second and weaker cooling periods is observed in November–January. During this period, the warming by net surface heat flux decreases following the weakening of shortwave radiation. It is combined with strong cooling by horizontal advection around −36 W m^{-2}.

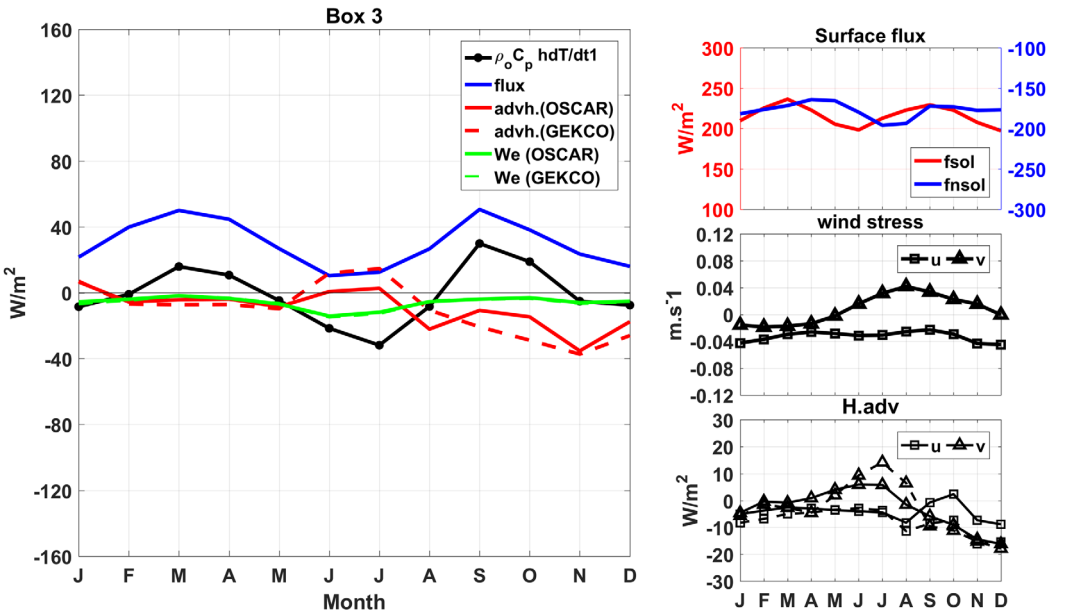

Figure 9. Same as Figure 7, but for box 3.

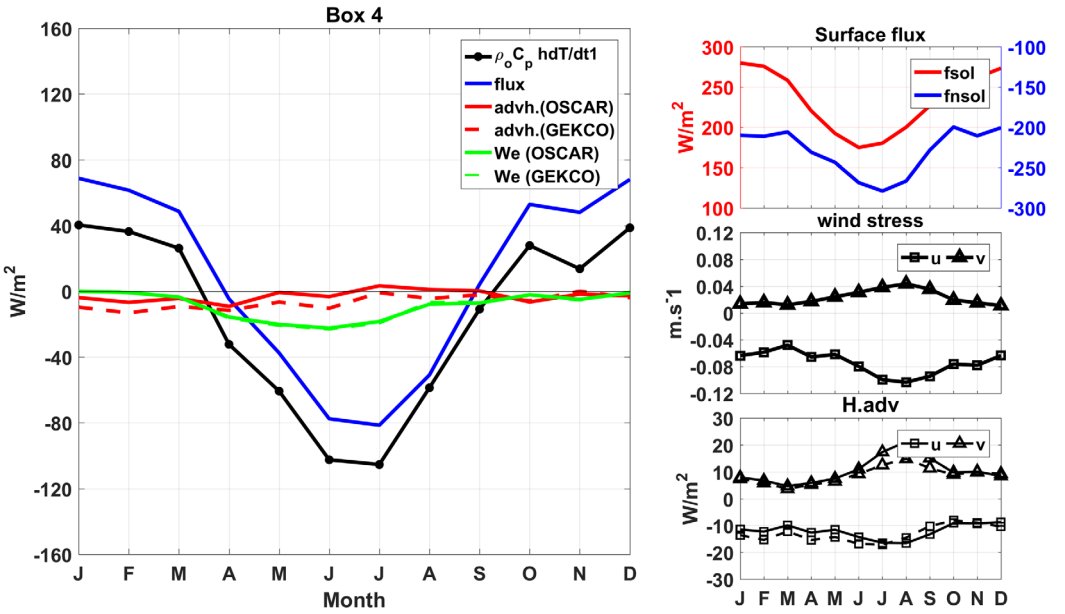

Figure 10. Same as Figure 7, but for box 4.

The warming by Hadv during boreal summer can be related to meridional advection of warm waters due to the intensification of zonal currents. Additionally, in regions north of 5°N and west of 35°W, warming can be related to an important input of warm and low-salinity waters from the Amazon river by the NBC retroflection (Ffield, 2005; Nogueira Neto & Silva, 2014; Wilson et al., 2002). From September to November, a relatively strong negative Hadv is observed (20–40 W m^{-2}). This can be related to an intensification of the southward advection of relatively cold waters from the northern Atlantic basin. This occurs after intensification of northeasterly trade winds not far from 5°N and westward advection of cold waters from the ACT region.

4.2.3. Southwestern Tropical Atlantic (Box 4)

In box 4, surface fluxes drive the seasonal cycle of SSTs (Figure 10). This term has almost the same magnitude as in the north hemisphere counterpart (box 1), but in box 4 it seems to be more efficient to imprint the variability of the mixed-layer heat content (Figure 10).

This region shows a period of strong cooling from April to September with values around −80 W m^{-2}. It is strongly related to a decrease of heating by shortwave radiation combined with an increase in latent heat loss due to southeasterly intensification. The warming period is observed from October to March with a maximum of 40 W m^{-2} which is twofold higher than in the northern boxes. This period is mainly driven by an increase of heating by shortwave radiation which is relatively stronger than the decrease of latent heat loss.

Oceanic contribution to the heat storage by Hadv and entrainment are weak and negative throughout the year (Figure 10). Only a relatively weak increase in cooling by entrainment is observed during a boreal summer, reaching 20 W m^{-2}. Oceanic contributions are extremely weak during boreal winters in this region, when stratification is higher and MLD is around 40 m depth (not shown). MLDs deepen in boreal summer (not shown), mainly in the southern part of this box, indicating less stratification and favorable condition for vertical mixing, which contributes to stronger cooling in the southern box compared with the northern ones.

4.2.4. Seasonal Cycle of the Residual Term

The seasonal cycle of the corrected RES presents an important contribution to the heat budget reaching values of around −40 W m^{-2} (Figure 11). In this section, we investigate the regions and periods where RES can be related to physical processes based on oceanic and atmospheric contexts and previous studies. Each box are investigated in order to identify when and where the residual term can be associated with vertical mixing.

During November–February in box 1 and December–January in box 2 RES presents positive values which means that the residual is essentially driven by accumulated errors of all terms of the heat budget. As a consequence no physical signal can be extracted from RES, in particular the vertical mixing. On the other hand,

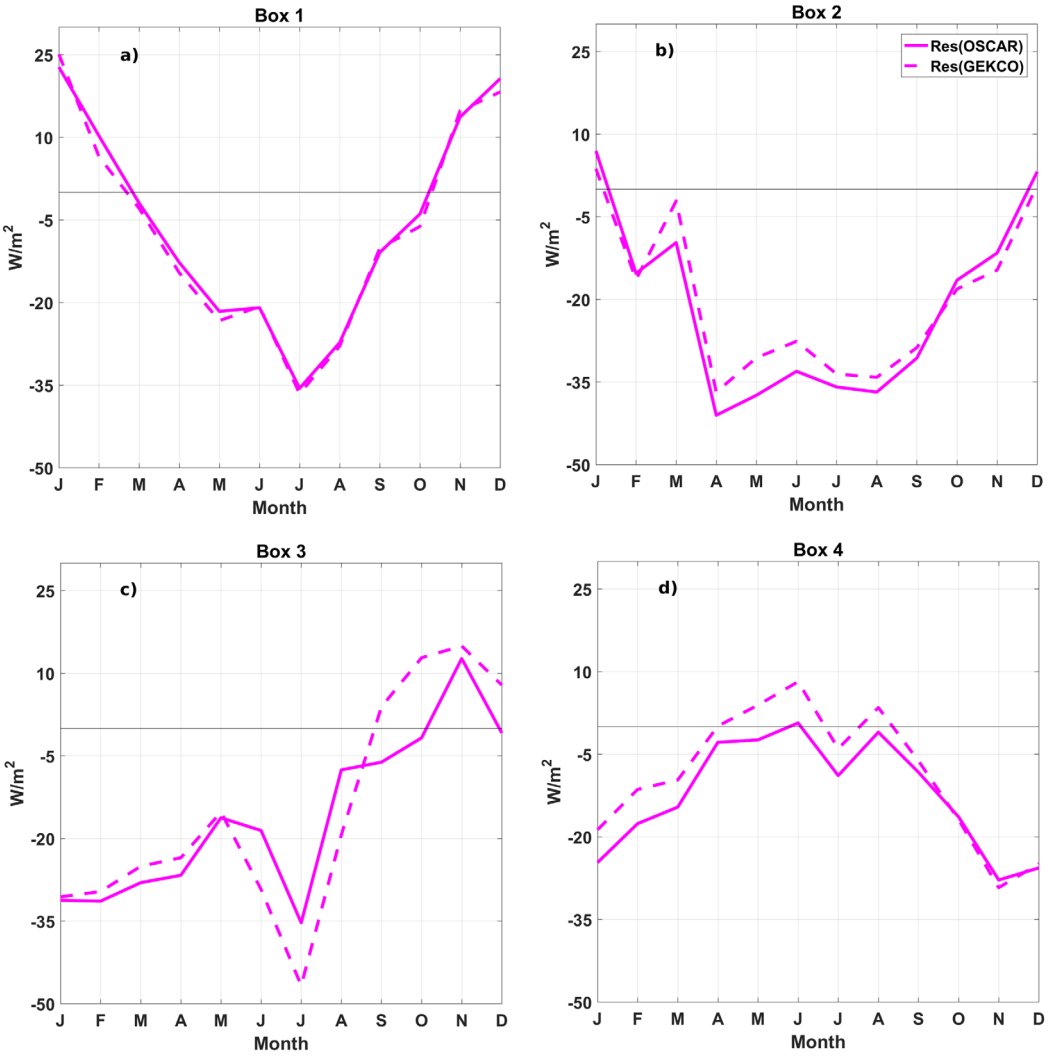

Figure 11. Mean seasonal cycle of the residual term in each box.

during boreal springs and summers, RES displays negative values comparable to vertical processes estimated by Servain and Lazar (2010) and Foltz et al. (2013) (Figures 11a and 11b).

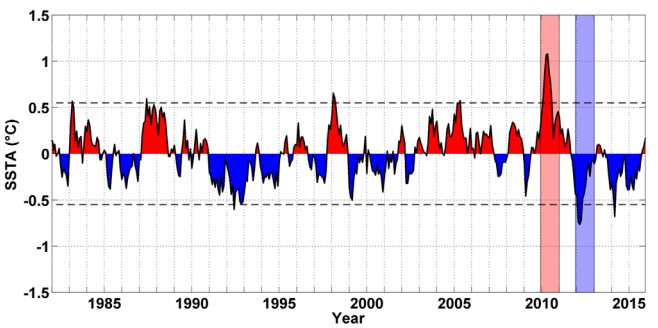

Figure 12. Monthly mean SST anomalies with respect to 1982–2012 reference period. The series of WTA averaged SSTs has been deseasonalized and detrended over the reference period. Read and blue shaded bars highlight the 2010 and 2012 years, respectively. Dotted lines represents $\pm 2\sigma$ (standard deviation) of the series.

In the eastern tropical Atlantic (28°W–18°W; 15°N–25°N), the monthly average of vertical processes, including entrainment and vertical mixing, obtained by Servain and Lazar (2010) and Foltz et al. (2013) well confirm the seasonal cycle of RES in boxes 1 and 2 shown in Figures 11a and 11b.

In the northern boxes, RES has negative values of around -40 W m^{-2} from April to September. During this period, the cooling due to vertical processes can be more efficient because the MLD becomes shallower (not shown). Foltz et al. (2013) have shown that vertical mixing intensifies during spring and summer when the barrier layer is thinner. Intensification of cooling by vertical processes can be explained by the occurrence of a vertical shear of the meridional velocity associated with an increase of the Ekman pumping which contributes in turn to the cooling of the surface layers. In box 2, the cooling in the cyclonic gyre of the Guinea Dome, south of Cape Verde Island even during the northernmost position of the ITCZ is induced by vertical mixing as already shown by Stramma and Schott (1999) and Servain and Lazar (2010).

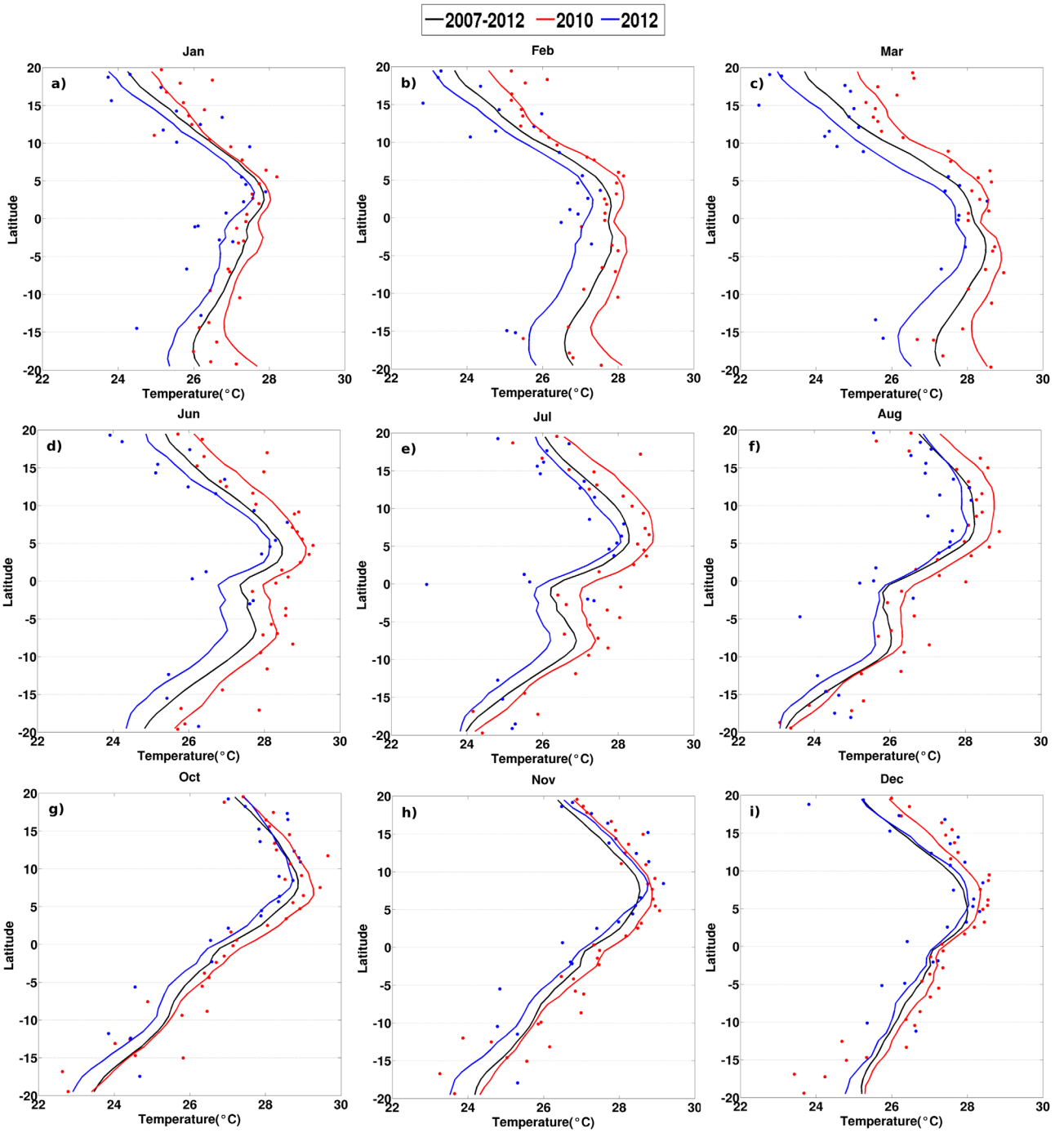

Figure 13. Monthly zonal averaged SSTr (solid lines) and $\overline{T}$ (dots) between 2010 (red), 2012 (blue), and the mean for the 2007–2012 period (black). Data were averaged every 1° of latitude.

Box 3 concerns a region of strong variability of currents. The seasonal intensification of surface currents in this zone is favorable to turbulent mixing. The influence of the seasonal variability of the NECC in the northern part of box 3 forms an intense eastward flow between the NEC and cSEC during a boreal summer and fall (Stramma & Schott, 1999) propitious to generating turbulence through vertical shear with equatorial undercurrents. RES shows negative values of around -25 W m^{-2} between January and May, and reaches -46 W m^{-2} from June to July. From September to December, RES displays positive values which have no physical meaning (Figure 11c).

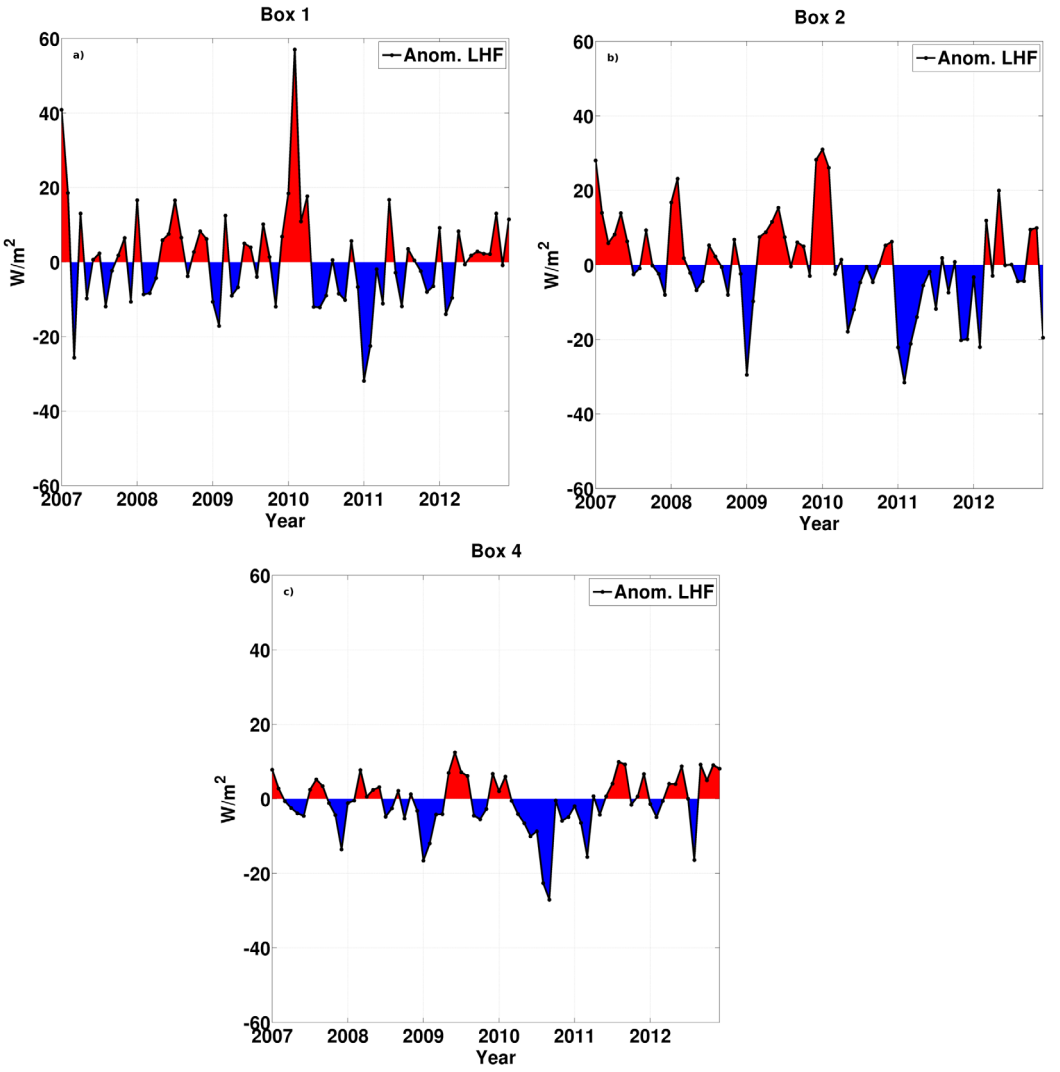

Figure 14. Latent heat flux anomalies from ERA-Interim colocated to Argo float profiles for each year from 2007 to 2012 in (a) box 1, (b) box 2, and (c) box 5.

In box 3, only the negative values observed in summer are comparable to maximum cooling by vertical processes as described in Peter et al. (2006) and Servain and Lazar (2010). During this period all terms contribute to the SST variability, but east of 30°W the cooling by vertical mixing dominates the SST drop during the summer (Hummels et al., 2014; Jouanno et al., 2011). At least during this period, despite the complexity and the large area considered, the RES term matches the intense oceanic circulations, which are favorable conditions to vertical mixing intensification.

In box 4, the residual term is close to zero and even slightly positive during boreal summers. From September to March, it reaches higher negative values (Figure 11d). Despite strong errors affecting the heat storage term (16 W m^{-2}, Table 5) and consequently RES in this region, the seasonal cycle of RES shown in Figure 11d is similar to that presented in Servain and Lazar (2010) for two boxes in the south tropical Atlantic (6°S–25°S; from the Brazilian coast to 30°W; and at 6°S–15°S; 30°W–10°E).

4.3. Interannual Variability: Comparison Between Years 2010 and 2012

In this section, the heat budget inferred from Argo floats is used to present evidence of causes of the monthly SST anomalies between the contrasted years 2010 and 2012. Figure 12 displays large SST anomalies observed in 2010 and 2012 in the WTA basin (the daily SSTr data were first averaged across the WTA basin, then converted into a monthly data series). These series were then deseasonalized and detrended

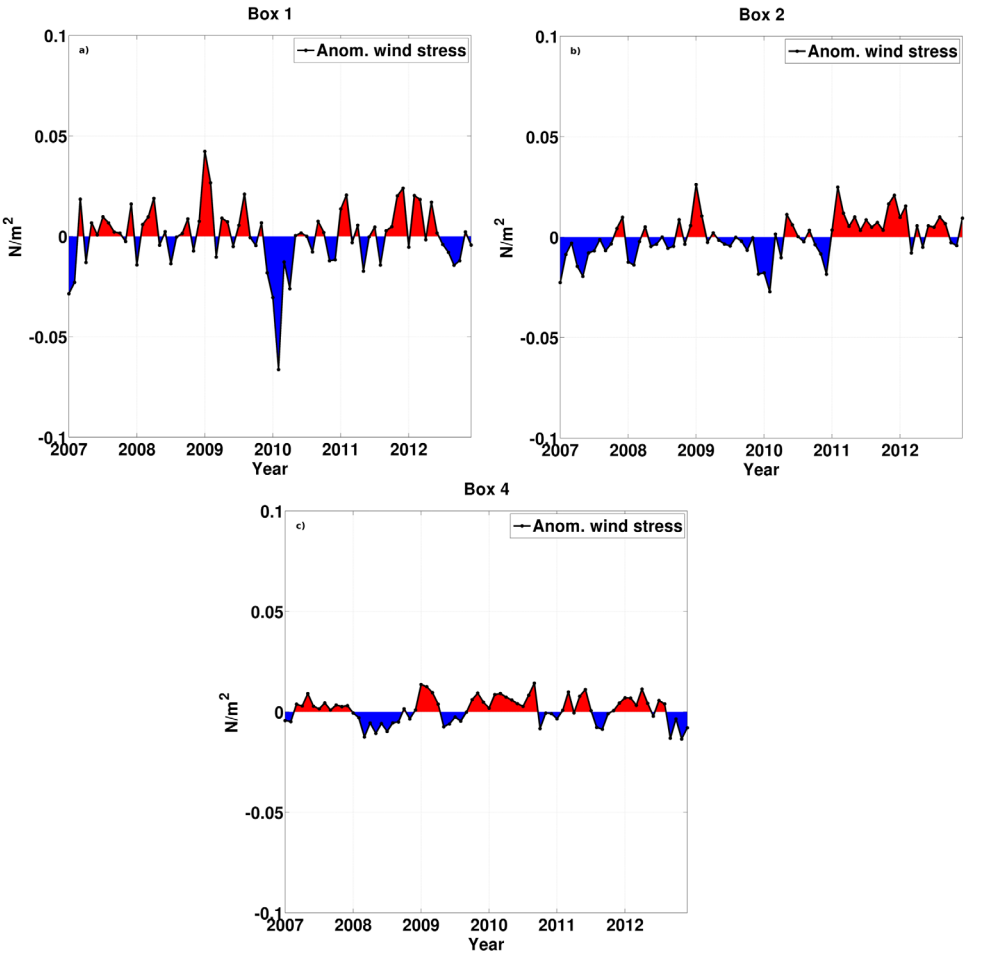

Figure 15. Wind stress anomalies from ERA-Interim colocated to Argo float profiles for each year from 2007 to 2012 in (a) box 1, (b) box 2, and (c) box 5.

over the reference period, 1982–2016. In 2010, positive SST anomalies were the strongest since 1982 reaching values of higher than 2σ in the series from March to August, while the negative SST anomalies observed in 2012 were the strongest during the reference period and reached high values ($+2\sigma$ of the series) between Mars and May.

The basin scale analysis of SST provides a general view of the interhemispheric comparisons for 2010 and 2012. Figure 13 displays a comparison between the latitudinal monthly SSTr of year 2010/2012 with the 2007–2012 period. The monthly latitudinal distribution of SSTr shows that SSTs in 2010 were higher than in 2012 by 1.6°C on average over the entire tropical Atlantic from February to August (Figures 13a–13f). The largest differences between years with respect to the 2007–2012 mean are found poleward of 10° during the January–March period. After August, SSTs tended to be closer to the mean of the period for both years. $\overline{T}$ values (blue and red points in Figure 13) agree well with SSTr; it is however important to underline the poor Argo sampling during 2012 in the southern hemisphere (fewer blue points in Figure 13).

Our diagnostics agree well with previous studies mentioning the existence of such SST anomalies during these 2 years (e.g., Ibánhez et al., 2016; Lefèvre et al., 2013; Marengo & Bernasconi, 2015; Marengo et al., 2013; Wang & Hu, 2016). These anomalies are present in all boxes but higher in the northern boxes (1 and 2) and the southern box (4). As these areas are mainly governed by the net surface fluxes, we present evidence of the causes of these SST anomalies based on monthly anomalies of the latent heat flux (Figure 14) and wind stress (Figure 15) colocated to Argo profiles. The monthly anomalies with respect to 6 years of observations (2007–2012) were taken as reference so as to provide an idea of the processes at the origin of the SST anomalies. These parameters show the importance of the previous years (2009 and 2011) in terms of

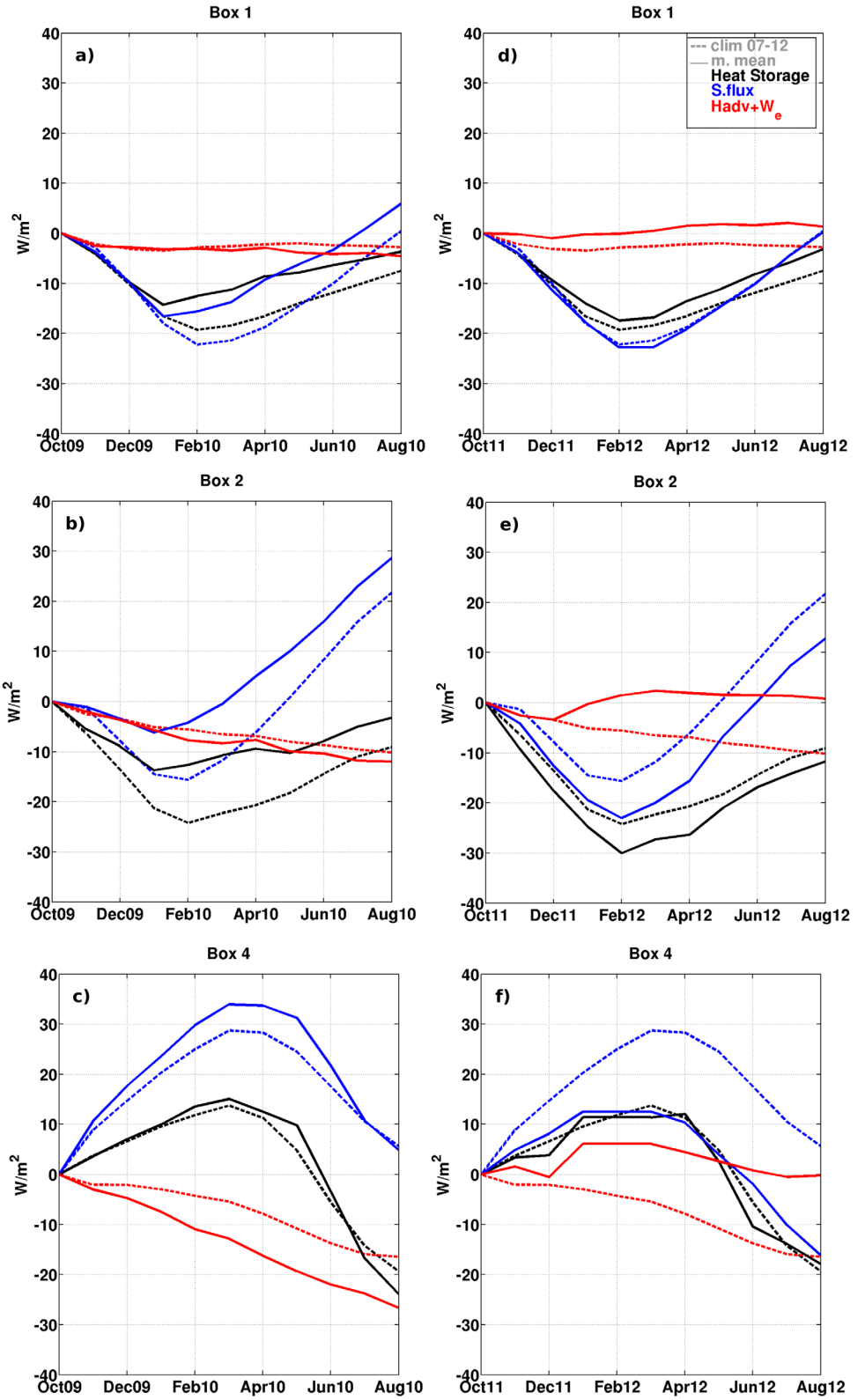

Figure 16. Accumulated heat budget for the period October–March (a–d) 2009/2010 and (e–h) 2011/2012. Local heat storage (black), surface flux (blue), and sum of oceanic terms (red). Dotted lines represent the mean for the 2007–2012 period.

the formation of such anomalies. Figure 16 displays the time-cumulation of heat storage, surface flux, and oceanic terms (sum of Hadv, W_e) from October to March 2009–2010 and 2011–2012 (this period concerns the period of generation of SSTs anomalies; see Figures 14 and 15). Additionally, in the western part of box 4 (west of 25°W) the heat storage mainly controlled by surface fluxes induces a pronounced cooling which explains well why SSTs were cooler than normal when observed in this region (Figure 13).

4.3.1. Anomalies in 2010

Between late 2009 and early 2010, the positive heat storage anomalies (not shown) are observed above 30 W m^{-2} in boxes 1 and 2. Positive anomalies in the latent heat flux around 50 W m^2 in boxes 1 and 2 and 10 W m^{-2} in box 4 (Figure 14) are at the origin of anomalous warming of the WTA surface waters. As displayed in Figure 15, these surface flux anomalies were generated by negative wind stress anomalies (down to -0.07 N m^{-2} in box 1, -0.03 in box 2, and -0.02 in box 4), meaning that the period between the end of 2009 and the beginning of 2010 experienced much weaker north-easterlies (south-easterlies) in the northern (southern) hemispheres than usual (Figure 16). The time-accumulated surface flux and heat storage term in boxes 1 and 2 present significantly reduced cooling from October 2009 to February 2010 (the cooling period in this region), while box 4 does not present significant warming during the same period (a warm season). The reduced heat loss during the cooling period in the northern tropical Atlantic (boxes 1 and 2; Figure 16) induces an earlier warming of the mixed layer, by 1 month in 2010, i.e., in February in the northern boxes, instead of March in the mean seasonal cycle (Figure 16). The weaker winds in 2010 led to a decrease of the wind-driven current intensification. Weaker horizontal advection therefore tends to cool the mixed layer, but not enough to balance the warming by surface flux.

4.3.2. Anomalies in 2012

In 2012, negative SST anomalies were mainly found in boxes 2 and 4. During the cooling period (the boreal winter of 2011–2012), the heat storage was about 20 W m^{-2} weaker than normal in the northeastern tropical Atlantic (box 2) (not shown). Again, these anomalies in both boxes are explained by negative surface heat flux anomalies, as a direct consequence of positive latent heat flux anomalies (Figure 14) and of positive wind stress anomalies, observed around 0.03 N m^{-2} from October 2011 to March 2012 (Figure 15). Intensities of wind stress anomalies in box 2 were generally weaker in 2011/2012 (maximum of 0.02 N m^{-2}) than in 2009/2010, but lasted all year long in 2011. In box 4, wind stress anomalies were around 0.02 N m^{-2} from October 2011 to June 2012 (Figure 15). The anomalously positive wind stress led to an excess of mixed-layer heat loss in box 2 which started in November 2011 (cooling period in this region; Figure 16e). In the western part of box 4, significant reduced warming by surface flux during October 2011 to April 2012 can be observed (warming period in this region) with an excess of heat loss between May and August (cooling period in the south; Figure 16f). During 2012, the positive wind stress anomalies led to a strong variability of surface currents in the tropical Atlantic, thus the horizontal advection had a relatively important contribution during this year. As shown in Figure 16f, the advection term tends to balance the surface flux term in box 4.

5. Summary and Conclusions

This study aimed at investigating the causes of the SST variability in the western tropical Atlantic (WTA). A mixed-layer heat budget was performed by using observations from Argo floats between 2007 and 2012, the best sampled period of this basin since the beginning of Argo deployments in 2000. Supplementary data, including satellite-derived SSTs, reanalysis of surface fluxes and current products were used to estimate the atmosphere and ocean forcing. An analysis of the mixed-layer heat budget components was conducted in four boxes (two northern boxes, one equatorial box, and one southern box), which covered the regional heterogeneities in the dynamics and thermodynamics of the WTA. Compared to gridded SSTr, the mixed-layer temperature calculated from Argo float profiles well represents the SST seasonal cycle during the period 2007–2012. This conclusion holds for the whole WTA, except for the first 5 months of the year in the northeastern region (box 2). Here a poor sampling in the upwelling region along the northwest African coast was found to be at the origin of such a discrepancy.

The relative contribution of each component to the heat budget was presented in terms of annual means and mean annual cycle in each box. First of all, positive values of the residual term were obtained to close the heat budget. As a consequence such residual term cannot be considered as mixing at the mixed-layer base because of a continuous decrease of temperature with depth. The strategy adopted to derive estimates of vertical mixing and its accuracy is based on an error analysis of each term of the mixed-layer heat

budget. This analysis has shown that the ECMWF ERA-I net surface heat flux is systematically affected by constant errors around 20 W m^{-2} across the entire tropical Atlantic which is confirmed by numerous works in all tropical regions. As a consequence, error on the net surface heat flux (20 W m^{-2}) was considered as negative bias used to derive a corrected net surface heat flux and finally a new residual term. It led to reasonably consistent and independent estimations of turbulent fluxes deduced from the residual and from a direct K-profile parameterization applied on the Argo floats. These two close and independent estimates validate the method proposed and give a good confidence of the vertical mixing deduced from corrected residuals. Errors in horizontal advection, due to uncertainties in current estimates (namely along the equator), entrainment and heat storage are much weaker, except for the heat storage term in box 4. They were not then taken into account because of their weakness and/or spatial intermittencies.

To conclude ERA-I surface heat fluxes were found to be under-estimated by 20 W m^{-2} and conducted to erroneous vertical mixing in the whole domain. Correction of these surface fluxes yielded to residuals which were assimilated to vertical turbulent mixing at the mixed-layer base. In year-mean averages, intensities obtained fell into realistic range.

On the other hand, the mean annual cycle of the residual still displays positive values and/or unrealistic trends in some boxes because of the cumulative errors which affect the other heat budget components. During October–February in boxes 1 and 2, for instance and from August to May in box 3, such spurious behavior highlights the limit of this methodology which provides retrievals of the heat budget components of poor and of even bad quality.

The seasonal evolution of all terms in each box agrees with previous studies, which concluded that the surface flux governs the SST variability poleward of 10°. In equatorial regions (box 3), it is also confirmed that the surface heat flux remains the most important term, but it is strongly balanced by horizontal advection during boreal spring and summer.

Considering previous studies (Foltz et al., 2013; Servain & Lazar, 2010), the vertical mixing is also an important process in open sea regions away from the equator, where the dynamics are weaker. This can be observed mainly in box 2 during a boreal spring and summer and in box 4 in boreal winter.

The interannual variability was analyzed by comparing 2010 and 2012 in terms of heat storage anomalies and surface fluxes and main related parameters. We highlighted the importance of 2009 and 2011 (later in this year) for anomalies observed in both years (2010 and 2012, respectively). For 2010, it was found that the warming period was anticipated for 1 month due to anomalous wind and latent heat flux during winter 2009–2010 in the northern tropical Atlantic. In 2012, the warm period is weaker than normal in box 2. Generally, the observed SST anomalies in 2010 and 2012 were generated by anomalous wind stress and, consequently, so was anomalous latent heat flux in the north Atlantic during winter. The wind-induced horizontal advection plays a fundamental role however in the balancing of the surface flux in the south Atlantic in 2012.

These results have shown that the north tropical Atlantic is a key region for the generation of the SSTs pattern observed in 2010 and 2012. Probably the ocean dynamics play an essential role in the maintenance of SSTs anomalies in both years. Model results could provide more precise information about this subject. Our results also confirmed the different behavior of the mixed-layer heat budget components within the tropical Atlantic. Despite the limitations in spatial and temporal scales Argo floats measurements, which led to errors in the heat storage estimations, we found that this Argo coverage can be extensively exploited. We think that this study is a first step of an advanced valorization of the Argo floats data which can be extended to other regions and other scientific issues.

An improvement in Argo array coverage mostly in the southern tropical Atlantic would be certainly an added value to better estimate and monitor the heat storage and underlying processes in the tropical Atlantic. Such estimates could be largely used as reference data to control and validate model outputs and reanalysis.

Acknowledgments
A.V.N.N. acknowledges the PhD scholarship support of the Sciences without Borders Program—Brazilian National Council for Scientific and Technological Development (CNPq grant 233680/2014-4). M.A. thanks the support of the Brazilian Research Network on Global Climate Change—Rede CLIMA (FINEP grant 01.13.0353-00). This paper is part of the Project Pôle d'Interaction pour une meilleure Lisibilité des études communes en Océanographie Tropicale atlantiquE—PILOTE (CNPq-IRD grant 490289/2013-4). The data used in this study can be made available upon request by contacting the corresponding author.

References

Araujo, M., Limongi, C. M., Servain, J., Silva, M. A., Leite, F. S., Veleda, D. R. A., et al. (2011). Salinity-induced mixed and barrier layers in the Southwestern tropical Atlantic Ocean off the Northeast of Brazil. *Ocean Science*, *7*, 63–73.

Ayina, L., & Bentamy, A. (2006). The impact of satellite winds and latent heat fluxes in a numerical simulation of the tropical Pacific Ocean. *Journal of Climate*, *19*, 5889–5902.

Bonjean, F., & Lagerloef, G. S. E. (2002). Diagnostic model and analysis of surface current in tropical Pacific. *Journal of Physical Oceanography*, *32*, 2938–2954.
Bourlès, B., Molinari, R. L., Wilson, W. D., & Leaman, K. D. (1999). Upper currents in the westerns tropical Atlantic (1989–1991). *Journal of Geophysical Research*, *104*, 1361–1376.
Caniaux, G., Giordani, H., Redelsperger, J.-L., & Guichard, F. (2011). Coupling between the Atlantic cold tongue and the west African monsoon in boreal spring and summer. *Journal of Geophysical Research*, *106*, C04003. https://doi.org/10.1029/2010JC006570
Caniaux, G., Prieur, L., Giordani, H., & Redelsperger, J.-L. (2017). An inverse method to derive surface fluxes from the closure of oceanic heat and water budgets: Application to the north-western Mediterranean Sea. *Journal of Geophysical Research: Oceans*, *122*, 2884–2908. https://doi.org/10.1002/2016JC012167
Cintra, M., Lentini, C. A. D., Servain, J., Araújo, M., & Marone, E. (2015). Physical processes that drive the seasonal evolution of the Southwestern Tropical Warm Pool. *Dynamic of Atmospheres and Oceans*, *72*, 1–11.
de Boyer Montégut, C., Madec, G., Fishier, A. S., & Lazar, A. (2004). Mixed layer depth over the global ocean: An examination of profile data and a profile-base climatology. *Journal of Geophysical Research*, *109*, C12003. https://doi.org/10.10292004JC002378
Dee, D. P., Uppala, S. M., Simmons, A. J., Berrisford, P., Poli, P., Kobayashi, S.., et al. (2011). The ERA-Interim reanalysis: Configuration and performance of the data assimilation system. *Quarterly Journal of the Royal Meteorological Society*, *137*, 553–597. https://doi.org/10.1002/qj.828
De Mey, P., & Ménard, Y. (1989). Synoptic analysis and dynamical adjustment of GOES-3 and SEASAT altimeter eddy fields in the northwest Atlantic. *Journal of Geophysical Research*, *94*, 6221–6230.
Ffield, A. (2005). North Brazil current rings viewed by TRMM microwave image SST and the influence of Amazon plume. *Deep-Sea Research Part I*, *52*, 137–160. https://doi.org/10.1016/j.dsr.2004.05.013
Foltz, G. R., Grodsky, S. A., & Carton, J. A. (2003). Seasonal mixed layer budget of the tropical Atlantic Ocean. *Journal of Geophysical Research*, *108*(C5), 3146. https://doi.org/10.1029/2002JC001584
Foltz, G. R., Schmid, C., & Lupikin, R. (2013). Seasonal cycle of the mixed layer heat budget in the Northeastern Tropical Atlantic. *Journal of Climate*, *56*, 8169–8188. https://doi.org/10.1175/JCLI-D-13-00037.1
Giordani, H., & Caniaux, G. (2011). Diagnosing vertical motion in the Equatorial Atlantic. *Ocean Dynamic*, *61*, 1995–2018.
Giordani, H., Caniaux, G., & Voldoire, A. (2013). Intraseasonal mixed-layer heat budget in the equatorial Atlantic during the cold tongue development in 2006. *Journal of Geophysical Research*, *118*, 650–671. https://doi.org/10.1029/2012JC008280
Hastenrath, S. (1984). Interannual variability and annual cycle: Mechanisms of circulation and climate in tropical Atlantic sector. *Monthly Weather Review*, *12*, 1097–1107.
Hastenrath, S. (2012). Exploring the climate problems of Brazil's Nordeste: A review. *Climate Change*, *112*, 243–251. https://doi.org/10.1007/s10584-011-0227-1
Hastenrath, S., & Greischar, L. (1993). Circulation mechanisms related to the northeast Brazil rainfall anomalies. *Journal of Geophysical Research*, *98*, 5093–5102.
Hidaha, K. (1956). Geostrophic currents and mixing. *Journal of the Oceanographic Society of Japan*, *12*, 109–110.
Hounsou-Gbo, G. A., Araújo, M., Bourlès, B., Veleda, D., & Servain, J. (2015). Tropical Atlantic contributions to strong rainfall variability along the northeast Brazilian coast. *Advances in Meteorology*, *2015*, 902084. https://doi.org/10.1155/2015/902084
Hummels, R., Dengler, M., & Brandt, P. (2014). Dyapcnal heat flux and mixed layer heat budget within the Atlantic Cold Tongue. *Climate Dynamics*, *43*, 3179–3199. https://doi.org/10.1007/s00382-014-2339-6
Ibánhez, J. S. P., Flores, M., & Lefèvre, N. (2016). Collapse of the tropical and subtropical North Atlantic CO_2 sink in boreal spring of 2010. *Scientific Reports*, *7*, 41694. https://doi.org/10.1038/srep41694
Jerlov, N. G. (1953). Studies of the equatorial currents in the Pacific. *Tellus*, *5*(3), 308–309. https://doi.org/10.3402/tellusa.v5i3.8590
Johns, W. E., Lee, T. N., Beardsley, R. C., Candela, J., Limeburner, R., & Castro, B. M. (1998). Annual cycle and variability of the North Brazil Current. *Journal of Physical Oceanography*, *28*, 103–128.
Johnson, E. S., Bonjean, F., Lagerloef, G. S. E., Gunn, J. T., & Mitchum, G. T. (2007). Validation and error analysis of OSCAR sea surface currents. *Journal of Atmospheric and Oceanic Technology*, *24*(4), 688–701.
Jouanno, J., Marin, F., Du Penhoat, Y., Sheinbaum, J., & Molines, J. M. (2011). Seasonal heat balance in the upper 100 m of the equatorial Atlantic Ocean. *Journal of Geophysical Research*, *116*, C09003. https://doi.org/10.1029/2010JC006912
Klinker, E. (1998). Diagnosis of the performance of the ECMWF model performance over the tropical oceans. *In Seminar on atmosphere-surface interaction* (pp. 53–66). Reading, UK: European Centre for Medium-Range Weather Forecasts.
Lefèvre, N., Caniaux, G., Janicot, S., & Gueye, A. K. (2013). Increasing CO_2 outgassing in February-May 2010 in tropical Atlantic following the 2009 Pacific El Niño. *Journal of Geophysical Research: Oceans*, *118*, 1645–1657. https://doi.org/10.1002/jgrc.20107
Lim, Y.-K., Schubert, S. D., Reale, O., Molodo, A. M., Suarez, M. J., & Auer, M. (2016). Large-scale controls on Atlantic cyclone activity on seasonal time scales. *Journal of Climate*, *29*, 6727–6749. https://doi.org/10.1175/JCLI-D-16-0098.1
Marengo, J. A., & Bernasconi, M. (2015). Regional differences in aridity/drought conditions over Northeast Brazil: Present state and future projections. *Climate Change*, *129*, 103–115. https://doi.org/10.1007/s10584-014-1310-1
Marengo, J. A., Soares, W. R., & Rodriguez, D. A. (2013). Two contrasting severe seasonal extremes in tropical south Atlantic in 2012: Flood in Amazonia and drought in Northeast Brazil. *Journal of Climate*, *26*, 9137–9154. https://doi.org/10.1175/JCLI-D_12_00642.1
Marin, F., Caniaux, G., Bourlès, B., Giordani, H., Guriou, Y., & Key, E. (2009). Why were sea surface temperatures so different in the eastern equatorial Atlantic in June 2005 and 2006? *Journal of Physical Oceanography*, *39*, 1416–1431. https://doi.org/10.1175/2008JPO4030.1
Merle, J., & Anoult, S. (1985). Seasonal variability of the surface dynamics topography in the tropical Atlantic ocean. *Journal of Marine Research*, *43*, 267–228.
Moore, D., & Philander, S. (1976). Modeling of the tropical oceanic circulation. *The Sea*, *6*, 319–361.
Nogueira Neto, A. V., & Silva, A. C. (2014). Seawater temperatures changes associated with the North Brazil current dynamics. *Ocean Dynamics*, *64*, 13–27. https://doi.org/10.1007/s10236-013-0667-4
Peter, A.-C., M., Le Hénaff, Y., Du Penhoat, C. E., Menkes, F., Marin, J., Vialard, G., et al. (2006). A model study of the seasonal mixed layer heat budget in the equatorial Atlantic. *Journal of Geophysical Research*, *111*, C06014. https://doi.org/10.1029/2005JC003157
Reynolds, R. W., Smith, T. M., Liu, C., Chelton, D. B., Casey, K. S., & Schlax, M. G. (2007). Daily high-resolution blended analyses for sea surface temperature. *Journal of Climate*, *20*, 5473–5496. https://doi.org/10.1175/2007JCLI1824.1
Schott, F. A., Stramma, L., & Fichier, J. (1995). The warmer water inflow in western Tropical Atlantic boundary regime, spring 1994. *Journal of Geophysical Research*, *100*, 24745–24760.
Servain, J. (1991). Simple climate indices for the Tropical Atlantic Ocean and some applications. *Journal of Geophysical Research*, *96*, 1537–1546.

Servain, J., & Lazar, A. (2010). Ocean dynamics contribution to seasonal mixed layer heat budget in the tropical Atlantic. In: Servain, J., Campos, J. N. B., Martins, E. S. B. R., & Reis, D. S. Jr. (Eds.), *Clima do Atlântico Tropical e Impactos Sobre o Nordeste do Brasil (CATIN)* (392 p.). Fortaleza, Brazil: FUNCEME/IRD, Editora Ronda.

Sodré, G. R. C., & Souza Filho J. D. C. (2013). Estudo de Caso: Análise sinótica de um evento extremo de precipitação no Estado de Pernambuco entre os dias 17 e 19 de Junho de 2010. *Revista Brasileira de Geofísica*, *6*, 66–78.

Sudre, J., Maes, C., & Graçon, V. (2013). On the global estimates of geostrophic and Ekman currents. *Limnology and Oceanography: Fluids Environments*, *3*.

Sudre, J., & Morrow, R. A. (2008). Global surface currents: A high-resolution product for investigating ocean dynamics. *Ocean Dynamics*, *58*, 101–118. https://doi.org/101007/s10236-008-0134-9

Sun, B., Yu, L., & Waller, R. A. (2003). Comparison of surface and turbulent heat fluxes over the Atlantic: NWP model analysis versus moored buoy observations. *Journal of Climate*, *16*, 679–695.

Stramma, L., & Schott, F. (1999). The mean flow field of Tropical Atlantic Ocean. *Deep-Sea Research Part II*, *46*, 279–303.

Thomson, R., & Fine, I. (2003). Estimating mixed layer depth from oceanic profile data. *Journal of Atmospheric and Oceanic Technology*, *20*, 319–329.

Vauclair, F., & Du Penhoat, Y. (2001). Interannual variability of the upper layer of the tropical Atlantic Ocean from in situ data between 1979 and 1999. *Climate Dynamics*, *17*, 527–546. https://doi.org/10.1007/s00380000125

Wade, M., Caniaux, G., & Du Penhoat, Y. (2011). Variability of the mixed layer heat budget in the eastern equatorial Atlantic during 2005–2007 as inferred using Argo floats. *Journal of Geophysical Research*, *116*, C08006. https://doi.org/10.1029/2010JC006683

Wagner, R. G. (1996). Mechanisms controlling variability of the interhemispheric sea surface temperature gradient in tropical Atlantic. *Journal of Climate*, *9*, 2010–2019.

Wang, M., & Hu, C. (2016). Mapping and quantifying *Sargassum* distribution and coverage in the central west Atlantic using MODIS observations. *Remote Sensing Environment*, *183*, 350–367. https://doi.org/10.1016/jrse.2016.05.019

Wilson, W. D., Johns, W. E., & Garzoli, S. L. (2002). Velocity structure of the North Brazil current rings. *Geophysical Research Letters*, *29*(8). https://doi.org/10.1029/2001GL013869

Yu, L., Jin, X., & Weller, R. A. (2006). Role of net surface heat flux in seasonal variations of sea surface temperature in the Tropical Atlantic. *Journal of Climate*, *19*, 6153–6169.

Yu, L., Waller, R. A., & Sun, B. (2004). Improving latent and sensible heat flux estimates for the Atlantic Ocean (1998–1999) by a synthesis approach. *Journal of Climate*, *17*, 373–393.